Human Antigen R-regulated mRNA metabolism promotes the cell motility of migrating neurons

Yi-Fei Zhao[1#], Xiao-Xiao He[1#], Zi-Fei Song[1], Ye Guo[2], Yan-Ning Zhang, Hua-Li Yu[1], Zi-Xuan He[1], Wen-Cheng Xiong[3], Wei-Xiang Guo*[2] and Xiao-Juan Zhu*[1]

[1] Key Laboratory of Molecular Epigenetics, Ministry of Education, Institute of Genetics and Cytology, Northeast Normal University, Changchun 130024 China

[2] State Key Laboratory for Molecular and Developmental Biology, Institute of Genetics and Developmental Biology, Chinese Academy of Sciences, Beijing 100101, China

[3] Department of Neurosciences, Case Western Reserve University, School of Medicine, Cleveland, OH 44106, USA

[#] These authors contributed equally

*Corresponding authors: zhuxj720@nenu.edu.cn; wxguo@genetics.ac.cn

Keywords: HuR, profilin1, neocortex development, neuronal migration, actin polymerization, mRNA metabolism

Abstract

Neocortex development during embryonic stages requires the precise control of mRNA metabolism. Human antigen R (HuR) is a well-studied mRNA binding protein that regulates mRNA metabolism, and it is highly expressed in the neocortex during developmental stages. Deletion of HuR does not impair neural progenitor cell proliferation or differentiation, but it disturbs the laminar structure of the neocortex. We report that HuR was expressed in postmitotic projection neurons during brain development. Specifically, depletion of HuR in these neurons led to a mislocalization of CDP^{+} neurons in deeper layers of the cortex. Time-lapse microscopy showed that HuR was required for the promotion of cell motility in migrating neurons. PCR array identified *profilin1* (*pfn1*) mRNA as a major binding partner of HuR in neurons. HuR positively mediated the stability of *pfn1* mRNA and influenced actin polymerization. Overexpression of Pfn1 successfully rescued the migration defects of HuR-deleted neurons. Our data revealed a posttranscriptional mechanism that maintains actin dynamics during neuronal migration.

Introduction

A correct laminar structure of the mammalian neocortex is essential to maintain proper brain function. Neuronal migration of cortical excitatory neurons (also known as projection neurons) is the key step in the establishment of the six-layers of neocortex during embryonic development (Kriegstein and Noctor, 2004; Sakakibara and Hatanaka, 2015; Sultan et al., 2013). Projection neurons follow an inside-out migration pattern to their final destinations in the cortex. Early-born neurons that possess a long leading process attach to the pial surface undergo somal translocation to establish the preplate (Nadarajah et al., 2001). Late-born neurons sequentially use three different migration modes, multipolar migration, glia-guided radial locomotion and terminal somal translocation, to reach the upper layer of the cerebral cortex (Rakic, 1972; Tabata and Nakajima, 2003). Neuronal migration is a highly complex and dynamic process that may require several days to complete in the mouse brain. Numerous factors regulate this process, such as cytoskeletal, cell adhesion and cell signaling molecules (Ayala et al., 2007; Ohtaka-Maruyama and Okado, 2015). However, mRNA metabolism, which is a fundamental cellular process that contributes to the generation of all of the aforementioned cellular molecules, is not well-studied in neuronal migration.

The RNA-binding proteins (RBPs) are key to the spatiotemporal orchestration of mRNA fate and mediate mRNA splicing, transportation, stability, and translation (Darnell, 2013; Lebedeva et al., 2011). Human antigen R (also known as ELAVL1) is a ubiquitously distributed member of the Hu family. HuR was estimated to have 26,000 transcriptome-wide targets in different cell lines, and it was implicated in multiple steps of posttranscriptional mRNA processing (Katsanou et al., 2005; Lebedeva et al., 2011; Mukherjee et al., 2011). HuR-mediated mRNA metabolism was implicated in neuron protection (Skliris et al., 2015), neurodegeneration disease (Lu et al., 2009; Vanderweyde et al., 2013), synaptic function (Yokoi et al., 2017), depression (He et al., 2019) and adult neurogenesis (Wang et al., 2019) in the adult mouse brain. In contrast, the role of HuR in the developing mouse brain is not well studied, which may be due to lethality in HuR-deleted embryos. Recent studies showed that conditional knockout of HuR in the telencephalon during embryonic development impaired proper neocortex formation (Kraushar et al., 2014, Popovitchenko et al., 2016). Wang and colleagues also showed that HuR had no impact on the proliferation and

differentiation of neural progenitor cells (NPCs) (Wang et al., 2019). Therefore, the physiological role of HuR in developing neurons remains obscure.

We found that HuR expression in postmitotic neurons contributed to the laminar structure of the mouse brain. *In utero* electroporation and time-lapse microscopy techniques were used and discovered a specific role of HuR in the regulation of cell motility of migrating neurons. PCR array screening identified the mRNA of *profilin1* (*pfn1*) as a major binding partner of HuR. Biochemical studies confirmed that HuR regulated the stability of *pfn1* mRNA, which influenced the F/G-actin ratio in neurons. Notably, Pfn1 overexpression rescued cell motility defects in HuR-deleted neurons. These data showed a critical role of HuR in the regulation of neuronal migration during brain development.

Results

HuR in post-mitotic projection neurons regulates corticogenesis

HuR had peak protein levels from E15.5 to E17.5 in the developing mouse neocortex (Fig. 1A), which was consistent with the high mRNA levels of HuR from E13.5 to E15.5 (Fig. 1B) because a two-day delay is often observed for corresponding mRNA and protein levels in the developing cortex (DeBoer et al., 2013; Kwan et al., 2012). Immunostaining result showed a ubiquitous distribution of HuR in the developing brain, with a stronger staining signal in the cortical plate (CP) (Fig. 1C). Previous studies showed that deletion of HuR disturbed lamination of the mouse neocortex (Kraushar et al., 2014, Popovitchenko et al., 2016), which could result from defects in neurogenesis or neuronal migration. Wang and colleagues recently reported that HuR conditional knockout (KO) by EMX1-Cre did not impair neurogenesis during mouse embryonic development (Wang et al., 2019). Therefore, we first examined proliferation and differentiation of neural progenitor cells (NPCs) in $HuR^{fl/fl}$; Nestin-Cre mice. Nestin-Cre mediates recombination in all types of neural progenitor cells and should have a broader effect than EMX1-Cre-mediated gene knockout (Giusti et al., 2014). BrdU labeling was performed at E14.5, and brain slices were analyzed at 2 h and 48 h. The ratios of $PAX6^+$ $BrdU^+$ and $Tbr2^+$ $BrdU^+$ cells among the total $BrdU^+$ cells were similar

between $HuR^{fl/fl}$; Nestin-Cre mice and $HuR^{fl/fl}$ mice 2 h post-BrdU injection (Fig. S1A-E). The ratio of $Tbr1^+$ $BrdU^+$ cells among total $BrdU^+$ cells was also similar between the two mouse brains 48 h post-BrdU injection (Fig. S1F-G). Therefore, HuR most likely functions in post-mitotic neurons to contribute to neocortical lamination. Consistent with this hypothesis, we found that HuR was highly co-localized with DCX, a marker of immature neurons, in the E16.5 developing brain (Fig. 1C). To specifically address the roles of HuR in these neurons, we crossed $HuR^{fl/fl}$ mice with NEX-Cre mice, in which Cre mediates recombination in post-mitotic projection neurons (Goebbels et al., 2006). NEX-Cre-mediated expression was confirmed in brain sections of a reporter mouse (Ai27D; NEX-Cre) (Fig. S2A). Therefore, the $HuR^{fl/fl}$; NEX-Cre mice should lack HuR expression in post-mitotic projection neurons beginning on E11.5 (Goebbels et al., 2006). A substantial decrease in the HuR protein level was detected in cortical lysates of P0 $HuR^{fl/fl}$; NEX-Cre mice (Fig. S2B), and HuR was absent from CDP^+ and $CTIP2^+$ neurons (Fig. S2C), which are markers of mature cortical neurons. These data confirmed the HuR knockout efficiency and specificity in $HuR^{fl/fl}$; NEX-Cre mice.

Using this mouse model, we studied cortical lamination via co-staining of DAPI with CDP, CTIP2 or FOXP2 in P28 mouse cortical sections. No differences in total cortical thickness were detected, but a significant decrease in layer II-IV thickness (defined by DAPI staining) was observed in $HuR^{fl/fl}$; NEX-Cre mice (Fig. 1 D and E). Consistently, a reduction in CDP^+ layer thickness was observed in $HuR^{fl/fl}$; NEX-Cre mice (Fig. 1 D and F), but not for other markers (Fig. S2 D). The distributions of CDP^+, $CTIP2^+$ and $FOXP2^+$ cells were quantified in 10 arbitrarily defined layers along the cortex. Statistical analyses showed that substantially more CDP^+ cells were present in deeper layers (bin 5 and bin 7) of $HuR^{fl/fl}$; NEX-Cre mice compared to the control mice (Fig. 1F). CTIP2 and FOXP2 staining revealed no significant differences between the control and mutant mice (Fig. S2E and F). Therefore, cortical lamination was not properly established when HuR was absent from post-mitotic neurons.

HuR is essential for neuronal migration of late-born neurons

During corticogenesis, post-mitotic neurons follow an inside-out model to migrate to their final destinations (Molnár et al., 2010; Sekine et al., 2011). To further illustrate the role of HuR in neuronal migration, we used a BrdU birth-dating assay to compare the laminar position of $BrdU^+$ cells in E18.5 mutant mice and their control littermates. BrdU was administered at E12.5 to label early-born neurons (primarily localized in deeper layers) and at E15.5 to label late-born neurons (primarily localized in upper layers). No significant differences were observed in early-born neurons (Fig. 2A and B), but a significant proportion of late-born neurons failed to migrate to the upper layers and stayed in the deeper layers of the cortex (Fig. 2C and D). Therefore, HuR deletion primarily impaired the migration of late-born neurons, which is consistent with the lamination defect of the CDP^+ layer.

We then used the Cre-flox system to eliminate HuR in late-born neurons via *in utero* electroporation to verify the role of HuR in neuronal migration. RV-CAG-GFP-Cre (GFP-Cre) and RV-CAG-GFP-deltaCre (GFP-dCre) vectors that restricted the GFP localization in nuclei were electroporated into E15.5 $HuR^{fl/fl}$ cortices. A GFP-Cre vector was also electroporated into E15.5 WT cortices as a negative control. All mouse brains were analyzed at E18.5 to assess the distribution of GFP^+ cells. Quantification results showed that substantially more GFP^+ cells accumulated in the intermediate zone (IZ) and the ventricular/subventricular zone (VZ/SVZ) of HuR knockout (KO) brains than in those of the other two groups (Fig. 2E and F). Correspondingly, significantly fewer GFP^+ cells presented in the CP (represented by MAP2 staining) of HuR KO brains (Fig. 2G and H).

We constructed shHuR304 and shHuR686 plasmids to knockdown (KD) HuR expression in vivo, and a shNC was also constructed as a negative control. Western blotting analyses showed that shHuR686 had better knockdown efficiency than shHuR304 (Fig. S3A). Therefore, shHuR686 was used in the subsequent HuR KD experiments. The shNC or shHuR686 plasmid was electroporated into WT cortices at E15.5, and brain slices were analyzed at E18.5 (Fig. S3B). Quantification results showed a significant decrease in GFP^+ neurons in the CP and a concomitant increase in GFP^+ neurons in the IZ and VZ/SVZ in the

cortices transfected with shHuR686 compared to shNC (Fig. S3B-C). These data indicated that HuR played an essential role in neuronal migration.

HuR deficiency impairs the cell motility of migrating neurons

Late-born neurons follow a specific sequence of migration modes, including multipolar migration, glia-guided locomotion and terminal somal translocation, to arrive at their correct localizations. Because we found that HuR-deficient neurons accumulated in the IZ and VZ/SVZ, time-lapse microscopy was used to analyze the migration process of neurons. The GFP-2Acre vector, which allows GFP distribution throughout the cytoplasm, was electroporated into E15.5 WT and $HuR^{fl/fl}$ cortices to label late-born neurons. Live cortical slices were prepared at E17.5 to visualize the dynamic behaviors of GFP^+ neurons in the IZ (Fig. 3A and S4A). The total migration distance of neurons in an 8-h period decreased significantly in HuR-deleted neurons (Fig. 3B). However, the percentages of GFP^+ neurons that possessed a bipolar morphology were similar between the two electroporated groups (Fig. 3C). Because the multipolar-to-bipolar morphological transition is a critical step for migrating neurons in the IZ, we further analyzed the morphology of migrating neurons using a shRNA approach. The percentage of bipolar cells in the upper IZ (upIZ) and number of processes per cells in the lower IZ (loIZ) and upIZ were not significantly different between the shHuR686 and shNC groups (Fig. S4B-E).

We next performed an *in utero* electroporation assay at E15.5-E18.5 to investigate whether deletion of HuR affected neuronal migration in the CP. We specifically focused on GFP^+ neurons that had adopted bipolar morphology in the CP (Fig. 3D and S4F). The total migration distance of HuR^-deleted neurons was significantly shorter than that of control neurons (Fig. 3E). We also noticed significantly more static GFP^+ cells that did not move at all during the recording period in HuR-knockout cortices (Fig. 3F). These cells were not included in the calculation of total migration distance. The HuR-deleted neurons were inclined to the loss and regeneration of the leading process (Fig. 3G). These data suggested that the migration deficits in HuR KO neurons were due to the impairment of cell motility but not defects in morphological transition.

HuR binds to *profilin1* mRNA to promote Profilin1 expression

Because HuR is a well-studied mRNA binding protein, we used a mouse cell motility PCR array to identify target genes that exhibited altered expression levels in HuR KO neurons. Total RNA was extracted from cultured $HuR^{fl/fl}$ and WT NPCs infected with GFP-Cre lentivirus. Deletion of HuR in the infected cells was confirmed using immunostaining (Fig. S5A). The results showed that most of the detected genes were down-regulated, with a few exceptions of up-regulated genes (Fig. 4A and Table S1), which is consistent with the canonical function of HuR as an mRNA stabilizer. To validate this result, we used RNA-IP to confirm the binding of HuR with the target mRNAs (Fig. S5B). Except for the mRNA of *actn3*, most of the tested mRNAs were detected in the HuR binding complex (Fig. S5C). We also verified the mRNA expression levels of the top down-regulated (*actn1*, *fap*, *arf6* and *pfn1*) and up-regulated (*arhgef7*) genes in cortical samples. The results showed the expression levels of *arf6* and *pfn1* were significantly decreased, and the expression level of *arhgef7* was increased in HuR-deleted cortices, but the expression levels of *actn1* and *fap* were not significantly altered (Fig. S5D).

Among the most up-regulated and down-regulated genes, Pfn1 triggered our particular interest because it plays well-defined roles in regulating cell motility (Witke, 2004). The phenotypes of *pfn1* KO mouse neocortices were similar to those of $HuR^{fl/fl}$; NEX-Cre mice (Kullmann et al., 2011; Kullmann et al., 2012, Popovitchenko et al., 2016). We further verified a positive correlation between HuR and Pfn1 protein levels in HuR KO neurons and HuR KD NLT cells (Fig. 4B-D and Fig. S5E-G). Consistent with our RNA-IP results, the mRNA of *pfn1* precipitated with HuR protein (Fig. S5H). Therefore, HuR likely binds and stabilizes *pfn1* mRNA to promote Pfn1 expression. To test this hypothesis, HuR KO and control neurons were incubated with actinomycin D to inhibit mRNA synthesis, and the mRNA stability of *pfn1* was assessed over a 6-h period (Fig. 4E). The results showed that *pfn1* mRNA degraded in a time-dependent manner in HuR KO and control neurons (Fig. 4F). However, an almost 50% shorter half-life of *pfn1* mRNA ($T_{1/2}$ = 3.78 h in HuR KO cells versus $T_{1/2}$ = 7.56 h in WT cells) was found in HuR KO cells compared to that in control cells

(Fig. 4F). These results confirmed that HuR maintained *pfn1* mRNA stability to ensure proper protein expression in neurons.

The Hu protein family members, including HuR, recognize and bind AU-rich RNA elements (AREs) (Chen et al., 2002). We next investigated whether HuR directly bound with the *pfn1* mRNA 3′UTR and which part of the sequence was responsible for this binding. ARE sequence analysis was performed, and we cloned the full sequence of the *pfn1* mRNA 3′UTR and three truncated 3′UTRs, 3'UTR 1-81, 3′UTR 1-194 and 3′UTR 82-290, into a psiCheck2 luciferase reporter vector (Fig. 4G). Each construct was co-transfected with pCDH-HuR into HEK293T cells to assess the activity of luciferase, which was normalized to the same psiCheck2 vector that was co-transfected with pCDH. Significantly elevated luciferase activities were observed for the full *pfn1* mRNA 3′UTR and 3′UTR 82-290, and 3′UTR 1-81 and 3′UTR 1-194 did not produce this effect (Fig. 4H). Therefore, the latter part of *pfn1* mRNA 3′UTR was responsible for binding to HuR. Taken together, these data indicated that HuR was a direct stabilizer of *pfn1* mRNA, which enhanced the protein level of Pfn1 in neurons.

Profilin 1 rescues migration defects of HuR-deficient neurons

Pfn1 is a well-known actin-binding protein that regulates F-actin remodeling (Borisy, 2003; Carlsson et al., 1977; Mockrin and Korn, 1980; Witke, 2004), which is critical in the mediation of cell motility. Therefore, we performed protein fractionation of F-actin and G-actin to test whether the G/F actin ratio was altered in HuR KO neurons. An obvious decrease in F-actin was observed in HuR KO neurons (Fig. 5A-B), which confirmed that HuR was essential for F-actin dynamics in neurons. To validate whether the HuR-mediated actin polymerization defect depended on Pfn1, we constructed a Pfn1 expression vector (Pfn1) and confirmed Pfn1 expression in NLT cells using Western blotting (Fig. 5C). The genetic rescue experiment was first performed in NLT cells via co-electroporation of Pfn1 with the shHuR686 plasmid. The results showed that Pfn1 significantly rescued the F-actin deficit in HuR KD cells (Fig. S6A-B). We then co-electroporated the GFP-Cre plasmid with Pfn1 or control vector into $HuR^{fl/fl}$ cortices. The quantification results clearly showed that the distribution of GFP^{+} cells in the cortical slices of the Pfn1 rescue group was similar to that in

the control group (Fig. 5D and E). However, when Pfn1 was overexpressed alone in migrating neurons, an accumulation of GFP^+ cells in the IZ was observed (Fig. S5C-D).

We also performed time-lapse imaging to visualize whether Pfn1 overexpression improved the cell motility defects in HuR KO neurons. GFP-2Acre and Pfn1 expression vectors were co-electroporated into E15.5 $HuR^{fl/fl}$ cortices, and live cortical slices were prepared at E17.5 to analyze the dynamic behaviors of GFP^+ neurons in the IZ (Fig. 5F). As expected, the total migration distance of GFP^+ neurons in an 8-h period significantly improved (Fig. 5G), but the total migration distance of these neurons remained less than that of the WT control neurons. Considering the broad effect of HuR, we speculated that other downstream mRNAs were also involved in HuR regulation of neuronal migration. We further tested whether Arf6, which regulates migration speed in the IZ (Hara et al., 2016), rescued the migration defects in HuR-deficient neurons. The results showed that the co-expression of Arf6 did not improve the neuronal migration defects in HuR KO cells (Fig. S6E-G).

Collectively, our data provided evidence that Pfn1 was a major target of HuR in the regulation of cell motility of migrating neurons.

Discussion

The present study demonstrated that HuR was critical for neuronal migration to establish correct cortical lamination. Furthermore, we provided evidence that HuR mediated cell motility of migrating neurons via regulation of *pfn1* mRNA stability. These data described a previously undefined function of HuR during brain development.

Unlike other Hu protein family members (HuB, HuC and HuD) that are specifically expressed in the neural system, HuR is expressed in a wide range of cell types and mediates numerous biological events (Hinman and Lou, 2008). Global deletion of HuR caused the death of mouse embryos beyond mid-gestation (Katsanou et al., 2009), which suggests that HuR played an essential role during embryo development. However, when HuR was deleted in post-mitotic neurons (mediated by NEX-Cre) or in neuroepithelium cells (mediated by FOXG1-Cre), similar lamination defects were observed. Therefore, HuR primarily functions in post-mitotic neurons during neocortex development.

The proper migration of post-mitotic neurons is critical to establish correct cortical lamination (Rakic, 1972). We found that HuR deletion impaired proper cortex formation, which was shown by the reduced thickness of layers II-IV. In contrast, the deeper layers of the cortex were maintained. Consistent with these data, the BrdU birth-dating assays showed that the migration of late-born neurons (E15.5), but not early-born neurons (E12.5), impaired significantly. Two reasons may account for the differential roles HuR plays in early-born and late-born neurons. The protein levels of HuR were most prominent in E15.5 and E17.5 brains, which corresponds to the development of late-born neurons. Therefore, HuR should have a more sophisticated impact in these neurons. Notably, we found that the cortical lamination defects in $HuR^{fl/fl}$; Nex-Cre brains primarily resulted from the impaired cell motility of HuR KO neurons. During brain development, late-born neurons travel a much longer distance to arrive at their proper positions in the cortex. Therefore, the requirement for HuR-mediated cell motility was more imperative in these cells.

HuR-mediated cell motility has been well-documented in different cells due to different mechanisms (Chang et al., 2017; Cooper, 1991; Doxakis, 2014; Joseph et al., 2014). We verified *pfn1* mRNA as a binding partner of HuR in neurons. Pfn family members are pivotal in the promotion of actin dynamics at the plasma membrane to drive actin-linking processes (Carlsson et al., 1977; Witke, 2004). Pfn1 has been shown to regulate cell movement and morphogenesis (Carlsson et al., 1977; Tilney et al., 1983). Pfn1 regulates the size of the neocortex in the nervous system, but no detailed examination of cortical lamination was performed (Kullmann et al., 2011). We showed that Pfn1 played a major role in HuR-regulated cell motility because the overexpression of Pfn1 successfully rescued the migration defects in HuR KO neurons, and the overexpression of Arf6 did not produce this beneficial effect on neuronal migration. Moreover, Pfn1 overexpression alone had a deleterious effect on neuronal migration. Therefore, the precise control of *pfn1* mRNA during neuronal migration is crucial. Consistent with our data, HuR deficiency caused defects in migration rate and reduced the numbers of radial lamellipodia in Schwann cells, which resulted from Pfn1 down-regulation (Iruarrizaga-Lejarreta et al., 2012). In addition, HuR and Pfn1 are both involved in familial amyotrophic lateral sclerosis (Lu et al., 2009; Wu et al., 2012; Brettle et al., 2015; Matsye et al., 2017).

However, HuR, as an RNA-binding protein, may target hundreds of genes for post-transcriptional regulation at any given time. Other genes associated with cell motility may also be involved in the control of neuronal migration. In addition to *Pfn1* and *Arf6*, many other genes that appeared in the PCR array regulate neuronal migration. For example, Rac1 and Cdc42 are small GTPases that are required for precise control during neuronal migration because constitutively active and dominant-negative forms of Rac1 and Cdc42 significantly inhibited radial migration (Konno et al., 2005). The functions of these two molecules were primarily related to malformation of the leading process (Kawauchi et al., 2003; Kholmanskikh et al., 2005; Yang et al., 2012). Rnd3 is an atypical Rho GTPase that antagonizes RhoA activity during neuronal migration. Rnd3-silenced neurons exhibit enlarged leading processes and an excess of thin processes that extend from the cell body and the leading process (Pacary et al., 2011). These GTPases regulate the leading process of migrating neurons, but these phenotypic defects were not present in HuR-deficient neurons, which indicates that the functions of these GTPases did not overlap with HuR or Pfn1. Similar to Pfn1, several actin-binding proteins also play roles in neuronal migration. Myo10 is an nontraditional myosin family member that is involved in establishing proper migration orientation and the multipolar-to-bipolar morphology transition (Ju et al., 2014). The Arp2/3 complex is an actin nucleator that produces branched actin networks, and it is essential for the maintenance of radial glial cells (RGC) polarity and organization (Wang et al., 2016). Caveolin-1 regulates clathrin-independent endocytosis and elongation of the leading process (Shikanai et al. 2018). Cofilin disassembles actin filaments, and it is negatively regulated by the CDK5-p27 pathway. An appropriate balance of cofilin phosphorylation is required for proper cortical neuronal migration (Kawauchi et al., 2006). However, these phenotypic defects were not similar to our observations in HuR-deficient neurons and brains. Notably, the expression of most of the aforementioned genes was not significantly changed in our PCR array. Therefore, HuR may not regulate the mRNA stability of these genes, and these genes should not play significant roles in HuR-mediated neuronal migration.

In conclusion, our study revealed that HuR-mediated cell motility was essential for the development of the neocortex. These data extend the knowledge of the contribution of mRNA metabolism to brain development.

Materials and methods

Animals and cell lines

All mice used in this study were handled in accordance with the guidelines of the Institutional Animal Care and Use Committees of the Northeast Normal University, China. Females maintained on a 12-h light/dark cycle and were bred overnight with males. Noon on the day after breeding was considered E0.5. Wild-type mice that used in primary neuron cultured and in *in utero* electroporation are C57BL/6 background. $HuR^{fl/fl}$ mice (Stock No: 021431) and Ai27D (Stock No: 012567) were initially obtained from Jackson Laboratory and were maintained in C57BL/6 background. The NEX-Cre mice (Goebbels et al., 2006) and Nestin-Cre (Giusti et al., 2014) mice used in this study were kindly gifts from Dr. Zilong Qiu (institute of neuroscience, CAS, China). Genotyping of all mice were performed by PCR using primers listed in Table S2.

HEK293T cells were kindly provided by Stem Cell Bank, Chinese Academy of Sciences. NLT cells were stock of our lab, which were originally provided by Dr. Wencheng Xiong (Case Western Reserve University, USA). Both cells were cultured in Dulbecco's modified Eagle's medium supplemented with fetal bovine serum (FBS).

Plasmids

The RV-CAG-GFP-Cre, RV-CAG-GFP-deltaCre and RV-CAG-GFP-2ACre pCDH-CMV-GFP, pCDH-CMV-GFP-HuR, Lenti-GFP-Cre, Lenti-GFP-delta-Cre, pAX, pMD, and psiCheck2 plasmids are stocks of our lab. The shHuR686 was constructed from pGeneClip™ hMGFP backbone and used the following sequence: 5'-GTGGGATTTCTGGTGTCAATGTC-3'. The shHuR304was constructed from pGeneClip™ hMGFP backbone and used the following sequence: 5'-GTCATCAAAGATGCCAACTTAT-3'. The shNC was constructed from the same backbone plasmid with a randomized sequence that has no targets in mice genome. Plasmid of pCAGGS-Arf6-flag was kind gift from Dr. Sakagami (Kitasato University, School of Medicine). Plasmid of pCMV-SPORT6-profilin1 was purchased from Addgene. The truncated *pfn1* mRNA 3'UTR was constructed using following primers into psiCheck2. XhoI and NotI restriction sites are used for digestion and ligation. Sequences of cloning primers are listed in Table S2.

Antibodies

Primary antibodies included mouse anti-beta III Tubulin (1:1000, ab7751, Abcam), anti-β-actin (1:5000, A5316, sigma), rabbit anti-green fluorescent protein (GFP) (1:1000, ab6556, abcam), mouse anti-MAP2 (1:1000, M1406, Sigma-Aldrich), mouse anti-HuR (1:500, sc5261, Santa Cruz), rabbit anti-CDP (1:500, SC-13024, Santa Cruz), rat anti-CTIP2 (1:500, ab18465, abcam), rabbit anti-FOXP2 (1:500, ab16046, abcam), rabbit anti-GABA (1:500, A2052, Sigma), rabbit anti-Ki67 (1:500, RM-9106-S, Thermo Fisher Scientific), rabbit anti-Pax6 (1:200, PRB-278P, Covance Research), rabbit anti-Tbr2 (1:500, ab23345, Abcam), mouse anti-GAPDH (1:5000, TransGene Biotech), rat anti-BrdU (1:1000, ab6326, Abcam), rabbit anti-profilin1 (1:1000, abcam). Nuclei were stained with 4′,6-diamidino-2-phenylindole (DAPI) (Roche).

Western blotting

Fresh brain tissues, transfected HEK293T cells or infected cultured neurons were rinsed with phosphate buffered saline (PBS) 48h after transfection, and then homogenized in lysis buffer (RIPA: 20 mM Tris-HCl pH 7.4, 100 mM NaCl, 1% NP-40, 1 mM EDTA, 5 μg/ml aprotinin and 5 μg/ml leupeptin). Following addition of SDS sample buffer, samples were boiled for 5 min, equal amount of protein was subjected to SDS-polyacrylamide-gel electrophoresis (SDS-PAGE) and transferred to polyvinylidene difluoride membranes (Immobilon P; Millipore). Membranes were blocked using 5% bovine serum albumin that prepared in TBS-T (50 mM Tris-HCl, pH 7.4, 150 mM NaCl, 0.1% Tween-20) for 1 h at room temperature. Membranes were incubated with corresponding primary antibodies overnight at 4°C. Then membranes were washed three times with TBS-T, and were incubated with secondary antibody that conjugated to horseradish peroxidase for 1.5 h at room temperature. The blotted membranes were developed with AmershamTM ECLTM Prime Western Blotting Detection Reagent (GE Healthcare).

Standard PCR, Real-time PCR, and PCR array

The Standard PCR was performed as described previously (Wang et al., 2015). Briefly, each reaction contained 20-40 ng of cDNA (except the cDNA for the IP, for which 5% of the cDNA was used for each gene examined), 1U GoTaq DNA polymerase (Promega, #M3005), and 300 nM of forward and reverse primers (shown below) in a final reaction volume of 20 µl. Data analysis was done by the built in software of Tanon 1600.

Real time PCR and data analyses were performed according to SYBR Green PCR supermix (Bio-Rad, #172-5124) manufacturer's protocol by a Real-Time PCR System (Themo PIKOREAL 96). For data analyses, the relative expression level of each gene was normalized to internal controls of the same sample. The relative expression levels of genes between different samples were then calculated, while the expression level of each gene in control was set as 1.

For PCR array, 10 ng cDNA was added into each well of a mouse cell motility PCR array kit (Qiagen, PAMM-128Z). Each sample was applied to one array and independent duplicates were analyzed for WT and HuR KO samples. The sequences of qPCR primers used in this study are listed in Table S2.

Immunohistochemistry

Animals were transcardially perfused with 4% paraformaldehyde in PBS under anesthesia (0.7% pentobarbital sodium), and brains were fixed in 4% paraformaldehyde in 0.1 M phosphate buffer (pH 7.4) overnight and then placed in 35% sucrose in phosphate buffer saline (pH 7.4) overnight. Dehydrate samples were embedded in O.C.T. compound (Tissue-Tek) and then cryosectioned with a Leica cryostat CM1950. Immunostaining was performed with standard protocol.

Briefly, for staining, floating and sliced brain sections were first washed in PBS to remove cryoprotectant and then blocked in the PBS buffer containing 2% BSA and 0.2% triton-X

100, followed by incubation with primary antibodies diluted in PBS overnight in 4℃. After washing 3 times with PBST, secondary antibodies were incubated 1.5 h at room temperature. All sections were counterstained with DAPI

In utero electroporation

In utero electroporation was performed as previously described (Tabata and Nakajima, 2001). Briefly, pregnant mice were anesthetized, and their uterine horns were exposed with a midline laparotomy incision. Embryos were removed carefully and placed on humidified gauze pads. Plasmid DNA plus 0.01% Fast Green (Fluka) was injected into lateral ventricles of embryonic brains with a glass micropipette. A volume of 1 μL of shRNA plasmids (2 μg/μL) or expression constructs (2 μg/μL) was injected with plasmid that expressed chicken beta-actin promoter-enhanced green fluorescent protein (EGFP). For rescue experiments, expression constructs were co-injected with shRNA or Cre, and CAG-EGFP plasmids. The best rescue concentration was normally screened at mole ratio 2:1 and 1:1 (Cre vector to expression vector). The best rescue experiment was shown in the result and the mole ratio used for rescue was presented in the figure and figure legends.

For electroporation, 5 × 50 ms, 37 V square pulses separated by 950 ms intervals were delivered with forceps-type electrodes connected to an ECM 830 electroporator (BTX Harvard Apparatus). The uterus was then replaced into the abdominal cavity, and the abdomen wall and skin were sutured using a surgical needle and thread. The entire procedure was completed within 40 min. The pregnant mice warmed in an incubator until they regained consciousness, and embryos were allowed to develop *in utero* as experiment designed.

Time-lapse imaging

In utero electroporation was performed as described above at E15.5. Two days or three days after electroporation, embryonic brains were dissected in cold artificial cerebrospinal fluid. Brain slices (300 μm thick) were sectioned with a Leica Vibratome VT1000. To visualize neuronal migration, slices were transferred onto Millicell inserts (Millipore) in Neurobasal medium (Invitrogen) containing 2% B-27 supplement, 2 mM L-glutamine, and penicillin/streptomycin (50 μg/mL). The glass-bottomed dish was then fitted into a

temperature-controlled chamber on the microscope stage for 8 h at 37°C under a 5% CO_2 air atmosphere. Live-cell imaging was recorded every 20 min using an Olympus FV1000 laser scanning confocal microscope.

Isolation and analyses of NPCs

Embryo-derived NPCs were isolated from E15.5 $HuR^{fl/fl}$ mice and wild-type (WT) littermates and cultured as described before (Guo et al., 2012). Briefly, mouse cortex was dissected and placed in Hank's balanced salt solution (HBSS) on ice. Tissue was spin down and digested using PBS containing 0.125% (w/v) trypsin (Sigma). After dissociation with a fire-polished glass pipette, cells were filtered through a 70-μm cell strainer (BD Falcon, #252350, CA) and washed with HBSS, the single-cell suspension from each sample was collected and cultured in proliferating medium in a 5% CO_2 incubator at 37°C. Proliferating medium contained Neurobasal medium with B27 serum-free (Invitrogen, # 17504-044) and supplemented 20 ng/ml basic fibroblast growth factor (FGF-2; PeproTech, #K1606, Rocky Hill, NJ, USA), 20 ng/ml epidermal growth factor (EGF, PeproTech, #A2306), 1% Antibiotic-Antimycotic, and 2 mM L-glutamine. Half of the medium was replaced every two days.

Primary cortical neuronal cultures

Primary cortical neurons were cultured as described previously (Zhu et al., 2007). Briefly, embryonic (E16.5) cerebral cortex removed from pregnant mice were chopped into small pieces after the meninges were completely removed. After incubation in PBS containing 0.125% (w/v) trypsin (Sigma) for 20 min at 37°C, digested tissues were mechanically dispersed by repeated passaging through a Pasteur pipette in PBS containing 0.05% (w/v) DNase (Sigma). Dissociated cells were suspended in Neurobasal medium supplemented with B-27 (Life Technologies) and penicillin/streptomycin (100 U/ml) and were plated on poly-D-lysine coated dishes (Corning) to incubate at 37°C in a 5% CO_2 atmosphere.

Package of lentivirus

Briefly, lenti-viral DNA was co- transfected with packaging plasmids pMD and pAX into HEK293T cells using calcium phosphate method. The viral transfection vector DNA and packaging plasmid DNA were transfected into 5×15 cm dishes of cultured HEK293T cells using the calcium phosphate method. The medium containing lentivirus was collected at 36 and 60 hours post-transfection, pooled, filtered through a 0.2-μm filter, and concentrated using an ultracentrifuge at 20000 rpm for 2 hours at 4°C using a SW27 rotor (Beckman). The virus was washed once and then suspended in 100μl PBS.

RNA immunoprecipitation and *pfn1* RNA binding assay

RNA-IP was performed as describe before (Wang et al., 2015). Briefly, WT and HuR KO NPCs were harvested and homogenized in 1ml of ice-cold lysis buffer (10 mM Hepes (pH 7.4), 200 mM NaCl, 30 mM EDTA, and 0.5% Triton X-100) with 2×complete protease inhibitors (Roche, #11873580001). Nuclei and debris were pelleted at 3,000×g for 10min; the supernatant was collected and raised to 300 mM NaCl, and clarified at 14,000×g for 30min. The resulting supernatant was pre-cleared for 1h with 100μl recombinant protein G agarose (Invitrogen) (washed with lysis buffer first). An aliquot of pre-cleared input was saved for RNA extraction (200μl) and protein analysis (100μl). A monoclonal antibody against HuR was incubated with recombinant protein A dynabeads at 4ºC for 2h and washed 3 times with lysis buffer. RNase Inhibitors (Roche) were added to the remaining lysates. The pre-cleared lysates were immunoprecipitated with antibody-coated recombinant protein G agarose at 4ºC for 2 hours. After third wash with the lysis buffer, 10% of immunoprecipitate was saved for protein analysis. The remaining was washed one more time and was re-suspended by Trizol (Invitrogen, #15596018) for RNA isolation.

RNA binding assay was performed as previously described in Guo et al. 2018. Briefly, sequence of *pfn1* was amplified from pCMV-SPORT6-profilin1 using primers in Table S2. Then, the PCR fragment was ligated into pEASY-blunt3® vector (Transgene, CB301) in both directions (confirmed by DNA sequencing). Then both resultant vectors were linearized using SacI restriction enzyme to create anti-sense or sense templates for in vitro transcription.

Linearized vectors were in vitro transcribed using AmpliScritbeTM T7-FlashTM biotin-RNA transcription Kit (ASB71110, Epicentre Biotechnologies). To determine whether synthetic biotinylated *pfn1* RNA fragments could bind endogenous HuR, protein lysate was prepared by homogenizing mouse hippocampi using RIPA buffer (50 mM Tris–HCl pH 8, 150 mM NaCl, 1% NP-40, 0.5% sodium deoxycholate, 0.1% SDS). Then, 30 µg of purified biotinylated *pfn1* transcripts were incubated with 500 µg of total protein in the binding buffer (10 mM HEPES, pH 7.4, 3 mM MgCl2, 5% glycerol and 1 mM DTT) for 30 min at room temperature to allow the binding of biotinylated RNA and their binding proteins. Yeast transfer RNA (50 ng/ml) and heparin (5 mg/ml) were then added to the mixture to block non-specific binding and the binding reaction was allowed to continue for 10 more minutes. Dynabeads M-280 streptavidin (112-05D, Invitrogen) was then added to the mixture, and incubated with constant mixing overnight at 4 °C. To collect the protein bound by biotinylated *pfn1* RNA fragments, the beads were washed three times with 1x binding buffer and resuspended in 1x binding buffer with SDS gel loading dye to dissolve protein that bound to biotinylated *pfn1* RNA fragments. The proteins in the pulldown material were identified by Western blotting by using mouse anti-HuR antibody.

Actinomycin D treatment and mRNA stability assay

Culture $HuR^{fl/fl}$ cortical neurons were first infected with Lentivirus-Cre to knock-out HuR, then treated with 10 µg/ml of actinomycin D (Sigma-Aldrich, #A1410) to inhibit gene transcription as described before (Guo et al., 2011). Treated neurons were collected at designated time points for RNA isolation and real time PCR analysis. mRNA level of profilin1 was normalized to *gapdh*. RNA decay kinetics and half-life were analyzed using a published method (Bolognani et al., 2010; Perrone-Bizzozero et al., 1993). Briefly, for single rate decays we used the exponential function Mt=M0e-ƛt (Mt: amount of mRNA at t time, M0: amount of mRNA t t=0. ƛ=(ln2)/$T_{1/2}$ ($T_{1/2}$ is the half-life of the mRNA).

Luciferase reporter assay

Transfection of HEK293T was carried out using PEI according to the manufacturer's protocol. Briefly, 1×10^6/ml HEK293T were plated into 12-well plate for 24 hours. For transfection reagents setup, a total of 1μg DNA was added into 50μl opti-DMEM medium (Invitrogen, #11058-021) followed by the addition of 3μg PEI transfection reagent. The solution was mixed by pipetting 3-5 times, incubated for 20 minute, and then added into each well. 48 hours later, luciferase activity was detected using the Dual-Luciferase Reporter 1000 System (Promega, #E1980) based on the manufacturer's protocol. Briefly, collected cells were lysed in 100 μl of 1× passive lysis buffer at room temperature for 15 min. Then 20 μL of the lysate was added to 100 μl of Luciferase Assay Buffer II and mixed briefly. Firefly luciferase (F-luc) activity was immediately read using a SpectraMax® M2E plate reader (Molecular Devices Corp). Next, 100 μl of Stop & Glo Buffer with Stop & Glo substrate was added and mixed briefly. Renilla luciferase (R-luc) activity was immediately read. R-luc activity was normalized to F-luc activity to eliminate the variation of transfection efficiencies.

Calculation of the G/F-actin ratio.

The F/G-actin ratio was determined by Western blotting, as previously described (Huang et al., 2013). Briefly, the two forms of actin differ in that F-actin is insoluble, while G-actin is soluble. Primary cultured neurons that infected with lenti-virus or NLT cells that electroporated with indicated plasmids were homogenized in cold lysis buffer (10 mM K_2HPO_4, 100 mM NaF, 50 mM KCl, 2 mM $MgCl_2$, 1 mM EGTA, 0.2 mM DTT, 0.5% Triton X-100, 1 mM sucrose, pH=7.0) and centrifuged at 15,000 × g for 30 min. The actin components in the supernatant represented fraction of G-actin. The insoluble F-actin in the pellet was re-suspended in lysis buffer plus an equal volume of buffer 2 (1.5 mM guanidine hydrochloride, 1 mM sodium acetate, 1 mM $CaCl_2$, 1 mM ATP, and 20 mM Tris-HCl, pH=7.5) and incubated on ice for 1 h to convert F-actin into soluble G-actin, with gentle mixing every 15 min. The samples were centrifuged at 15,000 × g for 30 min. The actin components in this supernatant represented F-actin. Samples from the supernatant (G-actin)

and pellet (F-actin) fractions were proportionally loaded and analyzed by Western blotting using an anti-actin antibody.

Microscopy imaging and statistical analysis

For in utero electroporation assay, BrdU birth-dating assay and neuronal marker staining assay, the brain sections of the primary somatosensory cortex were observed by microscopes of Olympus FSX100 or Olympus FV1000 and analyzed by FV10-ASW 1.7 software (Olympus). Only the brightness, contrast, and color balance were optimized after acquisition. For in utero electroporation assay, a 500 μm wide cortical area was subject for cell counting and at least 100 GFP^+ cells would be counted in each section. For BrdU birth-dating assay and neuronal marker staining assay, a 200 μm wide cortical area was subject for cell counting and at least 150 stained cells would be counted in each section. Cell counting was performed in blinded fashion.

Cortical sub-regions were identified on the basis of cell density by using DAPI staining. The numbers of multipolar and bipolar cells, length of leading process and migration distance were counted with ImageJ software. Multipolar cells were defined as cells with more than 3 processes. For migration distance calculation, a migration tracing line was generated by connecting the center points of a given migrating neuron that presented in serial time-lapse images (60 min intervals). The total length of the migration tracing line was calculated by ImageJ software.

Statistical analysis was performed using Student's *t*-test and Mann-Whitney U test to compare the means of two groups, one-way analysis of variance (ANOVA) with *Bonferroni* post-hoc test was used to compare the means of multiple groups and two-way ANOVA with *Bonferroni* post-hoc analysis was used when two variables were included in one statistical analysis (GraphPad Prism and SPSS). Data were presented as the means ± standard error of the mean (SEM). * for $P < 0.05$, ** for $P < 0.01$, and *** for $P < 0.001$

Acknowledgements

We thank Dr. Hiroyuki Sakagami (Kitasato University School of Medicine, Japan) for providing the Arf6 expression plasmid.

Competing interests

The authors declare no competing interests.

Funding

This work was supported by the National Natural Science Foundation of China (31601128), the open funds of the State Key Laboratory of Medical Neurobiology, Jilin Provincial Key Laboratory of Neural Plasticity (20160622020JC), animal model platform of Jilin Province (20191008009TC), Program of International S and T Cooperation (2015DFA31580), and the Fundamental Research Funds for the Central Universities of China (2412019FZ025, 2412019FZ027). W.G. was funded by the Recruitment Program of the Global Youth Experts of China, 2015.

References

Ayala, R., Shu, T., and Tsai, L.H. (2007). Trekking across the brain: the journey of neuronal migration. *Cell* **128**, 29-43.

Bolognani, F., Tanner, D.C., Merhege, M., Deschênesfurry, J., Jasmin, B., and Perronebizzozero, N.I. (2010). In vivo post-transcriptional regulation of GAP-43 mRNA by overexpression of the RNA-binding protein HuD. *Journal of neurochemistry* **96**, 790-801.

Carlsson, L., Nyström, L.E., Sundkvist, I., Markey, F., and Lindberg, U. (1977). Actin polymerizability is influenced by profilin, a low molecular weight protein in non-muscle cells. *Journal of Molecular Biology* **115**, 465-483.

Chang, N., Ge, J., Xiu, L., Zhao, Z., Duan, X., Tian, L., Xie, J., Yang, L., and Li, L. (2017). HuR mediates motility of human bone marrow-derived mesenchymal stem cells triggered by sphingosine 1-phosphate in liver fibrosis. *Journal of Molecular Medicine* **95**, 1-14.

Chen, C.Y.A., Xu, N., and Shyu, A.B. (2002). Highly Selective Actions of HuR in Antagonizing AU-Rich Element-Mediated mRNA Destabilization. *Molecular & Cellular Biology* **22**, 7268-7278.

Chiaki, O.M., and Haruo, O. (2015). Molecular Pathways Underlying Projection Neuron Production and Migration during Cerebral Cortical Development. *Frontiers in neuroscience* **9**, 447**.**

Cooper, J.A. (1991). The Role of Actin Polymerization in Cell Motility. *Annual Review of Physiology* **53**, 585-605.

Darnell, R.B. (2013). RNA protein interaction in neurons. *Annual review of neuroscience* **36**, 243-270.

DeBoer, E.M., Kraushar, M.L., Hart, R.P., and Rasin, M.R. (2013). Post-transcriptional regulatory elements and spatiotemporal specification of neocortical stem cells and projection neurons. *Neuroscience* **248**, 499-528.

Doxakis, E. (2014). RNA binding proteins: a common denominator of neuronal function and dysfunction. *Neuroscience bulletin* **30**, 610-626.

Ghosh, M., Aguila, H.L., Michaud, J., Ai, Y., Wu, M.T., Hemmes, A., Ristimaki, A., Guo, C., Furneaux, H., and Hla, T. (2009). Essential role of the RNA-binding protein HuR in

progenitor cell survival in mice. *Journal of Clinical Investigation* **119**, 3530-3543.

Giusti, S.A., Vercelli, C.A., Vogl, A.M., Kolarz, A.W., Pino, N.S., Deussing, J.M., and Refojo, D. (2014). Behavioral phenotyping of Nestin-Cre mice: implications for genetic mouse models of psychiatric disorders. *Journal of psychiatric research* **55**, 87-95.

Goebbels, S., Bormuth, I., Bode, U., Hermanson, O., Schwab, M.H., and Nave, K.A. (2006). Genetic targeting of principal neurons in neocortex and hippocampus of NEX-Cre mice. *Genesis* **44**, 611-621.

Guo, W., Patzlaff, N.E., Jobe, E.M., and Zhao, X. (2012). Isolation of multipotent neural stem or progenitor cells from both the dentate gyrus and subventricular zone of a single adult mouse. *Nature Protocols* **7**, 2005-2012.

Guo, W., Zhang, L., Christopher, D.M., Teng, Z.Q., Fausett, S.R., Liu, C., George, O.L., Klingensmith, J., Jin, P., and Zhao, X. (2011). RNA-binding protein FXR2 regulates adult hippocampal neurogenesis by reducing Noggin expression. *Neuron* **70**, 924-938.

Guo, Y., Chen, X., Xing, R., Wang, M., Zhu, X., and Guo, W. (2018). Interplay between FMRP and lncRNA TUG1 regulates axonal development through mediating SnoN-Ccd1 pathway. *Human Molecular Genetics* **27**, 475-485.

Hara, Y., Fukaya, M., Hayashi, K., Kawauchi, T., Nakajima, K., and Sakagami, H. (2016). ADP Ribosylation Factor 6 Regulates Neuronal Migration in the Developing Cerebral Cortex through FIP3/Arfophilin-1-dependent Endosomal Trafficking of N-cadherin. *eNeuro* **3**, 1-20.

He, Z., Song, H., Liu, T., Ma, J., Xing, Z., Yin, Y., Liu, L., Zhang, Y., Zhao, Y., Yu, H., He, X., Guo, W., and Zhu, X. (2019). HuR in the Medial Prefrontal Cortex is Critical for Stress-Induced Synaptic Dysfunction and Depressive-Like Symptoms in Mice. *Cerebral Cortex*, **29**, 2737–2747

Hinman, M.N., and Lou, H. (2008). Diverse molecular functions of Hu proteins. *Cellular and molecular life sciences : CMLS* **65**, 3168-3181.

Huang, W., Zhu, P.J., Zhang, S., Zhou, H., Stoica, L., Galiano, M., Krnjevic, K., Roman, G., and Costa-Mattioli, M. (2013). mTORC2 controls actin polymerization required for consolidation of long-term memory. *Nature neuroscience* **16**, 441-448.

Joseph, R., Srivastava, O.P., and Pfister, R.R. (2014). Downregulation of β-actin and its regulatory gene HuR affect cell migration of human corneal fibroblasts. *Molecular Vision* **20**, 593-605.

Ju, X.D., Guo, Y., Wang, N.N., Huang, Y., Lai, M.M., Zhai, Y.H., Guo, Y.G., Zhang, J.H., Cao, R.J., Yu, H.L., et al. (2014). Both Myosin-10 isoforms are required for radial neuronal migration in the developing cerebral cortex. *Cereb Cortex* **24**, 1259-1268.

Katsanou, V., Papadaki, O., Milatos, S., Blackshear, P.J., Anderson, P., Kollias, G., and Kawauchi, T., Chihama, K., Nabeshima, Y.i., and Hoshino, M. (2003). The in vivo roles of STEF/Tiam1, Rac1 and JNK in cortical neuronal migration. *Embo Journal* **22**, 4190-4201.

Kawauchi, T., Chihama, K., Nabeshima, Y.I., and Hoshino, M. (2006). Cdk5 phosphorylates and stabilizes p27kip1 contributing to actin organization and cortical neuronal migration. *Nature cell biology* **8**, 17-26**.**

Kholmanskikh, S.S., Koeller, H.B., Wynshaw-Boris, A., Gomez, T., Letourneau, P.C., and Ross, M.E. (2006). Calcium-dependent interaction of Lis1 with IQGAP1 and Cdc42 promotes neuronal motility. *Nature neuroscience* **9**, 50-57.

Konno, D., Yoshimura, S., Hori, K., Maruoka, H., and Sobue, K. (2005). Involvement of the Phosphatidylinositol 3-Kinase/Rac1 and Cdc42 Pathways in Radial Migration of Cortical Neurons. *Journal of Biological Chemistry* **280**, 5082-5088.

Kontoyiannis, D.L. (2005). HuR as a negative posttranscriptional modulator in inflammation. *Mol Cell* **19**, 777-789.

Kraushar, M.L., Thompson, K., Wijeratne, H.R., Viljetic, B., Sakers, K., Marson, J.W., Kontoyiannis, D.L., Buyske, S., Hart, R.P., and Rasin, M.R. (2014). Temporally defined neocortical translation and polysome assembly are determined by the RNA-binding protein Hu antigen R. *Proceedings of the National Academy of Sciences of the United States of America* **111**, E3815-3824.

Kriegstein, A.R., and Noctor, S.C. (2004). Patterns of neuronal migration in the embryonic cortex. *Trends in neurosciences* **27**, 392-399.

Kullmann, J.A., Neumeyer, A., Gurniak, C.B., Friauf, E., Witke, W., and Rust, M.B. (2011). Profilin1 is required for glial cell adhesion and radial migration of cerebellar granule neurons. *EMBO reports* **13**, 75-82.

Kullmann, J.A., Neumeyer, A., Wickertsheim, I., Bottcher, R.T., Costell, M., Deitmer, J.W., Witke, W., Friauf, E., and Rust, M.B. (2012). Purkinje cell loss and motor coordination defects in profilin1 mutant mice. *Neuroscience* **223**, 355-364.

Kwan, K.Y., Lam, M.M., Johnson, M.B., Dube, U., Shim, S., Rasin, M.R., Sousa, A.M., Fertuzinhos, S., Chen, J.G., Arellano, J.I., et al. (2012). Species-dependent posttranscriptional regulation of NOS1 by FMRP in the developing cerebral cortex. *Cell* **149**, 899-911.

Lebedeva, S., Jens, M., Theil, K., Schwanhausser, B., Selbach, M., Landthaler, M., and Rajewsky, N. (2011). Transcriptome-wide analysis of regulatory interactions of the RNA-binding protein HuR. *Mol Cell* **43**, 340-352.

Linda, M., Tianyi, M., Henner, K., Jia-Min, Z., Antal, B., Shigeyoshi, F., Hsu, Y.W.A., Garcia, A.J., Xuan, G., and Sebastien, Z. (2012). A toolbox of Cre-dependent optogenetic transgenic mice for light-induced activation and silencing. *Nature neuroscience* **15**, 793.

Lu, L., Wang, S., Zheng, L., Li, X., Suswam, E.A., Zhang, X., Wheeler, C.G., Nabors, L.B., Filippova, N., and King, P.H. (2009). Amyotrophic lateral sclerosis-linked mutant SOD1 sequesters Hu antigen R (HuR) and TIA-1-related protein (TIAR): implications for impaired post-transcriptional regulation of vascular endothelial growth factor. *The Journal of biological chemistry* **284**, 33989-33998..

Mockrin, S.C., and Korn, E.D. (1980). Acanthamoeba profilin interacts with G-actin to increase the rate of exchange of actin-bound adenosine 5'-triphosphate. *Biochemistry* **19**, 5359-5362.

Molnár, Z., Métin, C., Stoykova, A., Tarabykin, V., Price, D.J., Francis, F., Meyer, G., Dehay, C., and Kennedy, H. (2010). Comparative aspects of cerebral cortical development. *European Journal of Neuroscience* **23**, 921-934.

Mukherjee, N., Corcoran, D.L., Nusbaum, J.D., Reid, D.W., Georgiev, S., Hafner, M., Ascano, M., Jr., Tuschl, T., Ohler, U., and Keene, J.D. (2011). Integrative regulatory mapping indicates that the RNA-binding protein HuR couples pre-mRNA processing and mRNA stability. *Mol Cell* **43**, 327-339.

Nadarajah, B., Brunstrom, J.E., Grutzendler, J., Wong, R.O.L., and Pearlman, A.L. (2001). Two modes of radial migration in early development of the cerebral cortex. *Nature neuroscience* **4**, 143-150.

Pacary, E., Heng, J., Azzarelli, R., Riou, P., Castro, D., Lebelpotter, M., Parras, C., Bell, D.M., Ridley, A.J., and Parsons, M. (2011). Proneural Transcription Factors Regulate Different Steps of Cortical Neuron Migration through Rnd-Mediated Inhibition of RhoA Signaling. *Neuron* **69**, 1069-1084.

Perrone-Bizzozero, N.I., Cansino, V.V., and Kohn, D.T. (1993). Posttranscriptional regulation of GAP-43 gene expression in PC12 cells through protein kinase C-dependent stabilization of the mRNA. *Journal of Cell Biology* **120**, 1263-1270.

Popovitchenko, T., Thompson, K., Viljetic, B., Jiao, X., Kontonyiannis, D.L., Kiledjian, M., Hart, R.P., and Rasin, M.R. (2016). The RNA binding protein HuR determines the differential translation of autism-associated FoxP subfamily members in the developing neocortex. *Scientific reports* **6**, 1-9.

Rakic, P. (1972). Mode of cell migration to the superficial layers of fetal monkey neocortex. *Journal of Comparative Neurology* **145**, 61.

Sakakibara, A., and Hatanaka, Y. (2015). Neuronal polarization in the developing cerebral cortex. Frontiers in neuroscience *9*, 116.

Sekine, K., Honda, T., Kawauchi, T., Kubo, K., and Nakajima, K. (2011). The outermost region of the developing cortical plate is crucial for both the switch of the radial migration mode and the Dab1-dependent "inside-out" lamination in the neocortex. *The Journal of neuroscience : the official journal of the Society for Neuroscience* **31**, 9426-9439.

Shikanai, M., Nishimura, Y.V., Sakurai, M., Nabeshima, Y.I., Yuzaki, M., and Kawauchi, T. (2018a). Caveolin-1 Promotes Early Neuronal Maturation via Caveolae-Independent Trafficking of N-Cadherin and L1. *iScience* **7,** 53-67.

Skliris, A., Papadaki, O., Kafasla, P., Karakasiliotis, I., Hazapis, O., Reczko, M.,

Grammenoudi, S., Bauer, J., and Kontoyiannis, D.L. (2015). Neuroprotection requires the functions of the RNA-binding protein HuR. *Cell death and differentiation* **22**, 703-718.

Sultan, K.T., Brown, K.N., and Shi, S.H. (2013). Production and organization of neocortical interneurons. *Frontiers in cellular neuroscience* **7**, 221.

Tabata, H., and Nakajima, K. (2001). Efficient in utero gene transfer system to the developing mouse brain using electroporation: visualization of neuronal migration in the developing cortex. *Neuroscience* **103**, 865-872.

Tabata, H., and Nakajima, K. (2003). Multipolar migration: the third mode of radial neuronal migration in the developing cerebral cortex. Journal of Neuroscience the Official *Journal of the Society for Neuroscience* **23**, 9996-10001.

Tilney, L.G., Bonder, E.M., Coluccio, L.M., and Mooseker, M.S. (1983). Actin from Thyone sperm assembles on only one end of an actin filament: a behavior regulated by profilin. *Journal of Cell Biology* **97**, 112.

Vanderweyde, T., Youmans, K., Liu-Yesucevitz, L., and Wolozin, B. (2013). Role of stress granules and RNA-binding proteins in neurodegeneration: a mini-review. *Gerontology* **59**, 524-533.

Wang, F., Tidei, J.J., Polich, E.D., Gao, Y., Zhao, H., Perrone-Bizzozero, N.I., Guo, W., and Zhao, X. (2015). Positive feedback between RNA-binding protein HuD and transcription factor SATB1 promotes neurogenesis. *Proceedings of the National Academy of Sciences of the United States of America* **112**, E4995-5004.

Wang, P.S., Chou, F.-S., Ramachandran, S., Xia, S., Chen, H.-Y., Guo, F., Suraneni, P., Maher, B., and Li, R. (2016). Crucial roles of the Arp2/3 complex during mammalian corticogenesis. *Development*, **143**, 2741-2752.

Wang, Y., Guo, Y., Tang, C., Han, X., Xu, M., Sun, J., Zhao, Y., Zhang, Y., Wang, M., Cao, X., et al. (2019). Developmental Cytoplasmic-to-Nuclear Translocation of RNA-Binding Protein HuR Is Required for Adult Neurogenesis. *Cell reports* **29**, 3101-3117 e3107.

Witke, W. (2004). The role of profilin complexes in cell motility and other cellular processes. *Trends in cell biology* **14**, 461-469.

Yang, T., Sun, Y., Zhang, F., Zhu, Y., Shi, L., Li, H., and Xu, Z. (2012). POSH localizes activated Rac1 to control the formation of cytoplasmic dilation of the leading process and neuronal migration. *Cell reports* **2**, 640-651.

Yokoi, S., Udagawa, T., Fujioka, Y., Honda, D., Okado, H., Watanabe, H., Katsuno, M., Ishigaki, S., and Sobue, G. (2017). 3'UTR Length-Dependent Control of SynGAP Isoform alpha2 mRNA by FUS and ELAV-like Proteins Promotes Dendritic Spine Maturation and Cognitive Function. *Cell reports* **20**, 3071-3084.

Zhu, X.J., Wang, C.Z., Dai, P.G., Xie, Y., Song, N.N., Liu, Y., Du, Q.S., Mei, L., Ding, Y.Q., and Xiong, W.C. (2007). Myosin X regulates netrin receptors and functions in axonal path-finding. *Nature cell biology* **9**, 184-192.

Figures

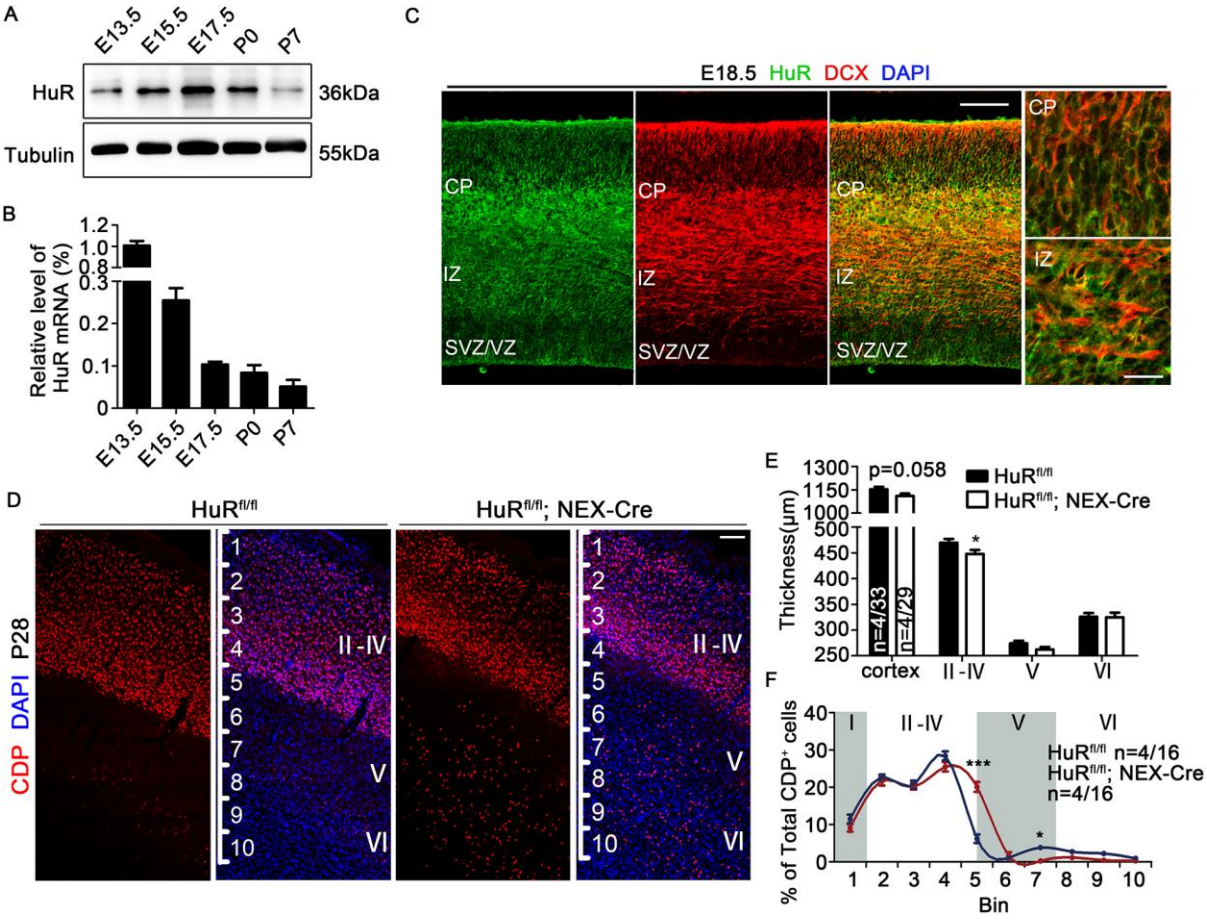

Fig. 1. HuR is expressed in post-mitotic neurons and regulates the laminar structure of the mouse neocortex. (A) Western blotting analyses of HuR protein expression in different neocortex samples. (B) Real-time PCR analyses of HuR mRNA expression in neocortex samples. Expression levels at E13.5 were set as 1. All experiments were performed three times in triplicate. (C) Immunostaining of HuR and DCX in E16.5 WT cortical sections. HuR highly co-localized with DCX in the developing brains. Scale bar=100 μm. Magnified images of the CP and IZ are shown in the right panel. Scale bar=20 μm. (D) Immunostaining of CDP in P28 $HuR^{fl/fl}$ and $HuR^{fl/fl}$; NEX-Cre cortical sections. Scale Bar=100 μm. Cerebral cortices were divided into 10 equal bins. Scale bar=100 μm. (E) Quantification of cortical layer thickness in $HuR^{fl/fl}$ and $HuR^{fl/fl}$; NEX-Cre cerebral cortices. Student's t-test was used for statistical analysis. The n values represent the numbers of brains/brain sections. (F)

Distribution of CDP^+ neurons in the cortex. Two-way ANOVA with *Bonferroni* post-hoc analysis was used for statistical analysis. The n values represent the numbers of brains/brain sections. For all images in this figure, nuclei were counterstained with DAPI. The numbers of brains and brain sections quantified in each experiment are indicated on the graphs. The data show the mean ± SEM. n.s.: $P > 0.5$; *: $P < 0.05$; **: $P < 0.01$; ***: $P < 0.001$.

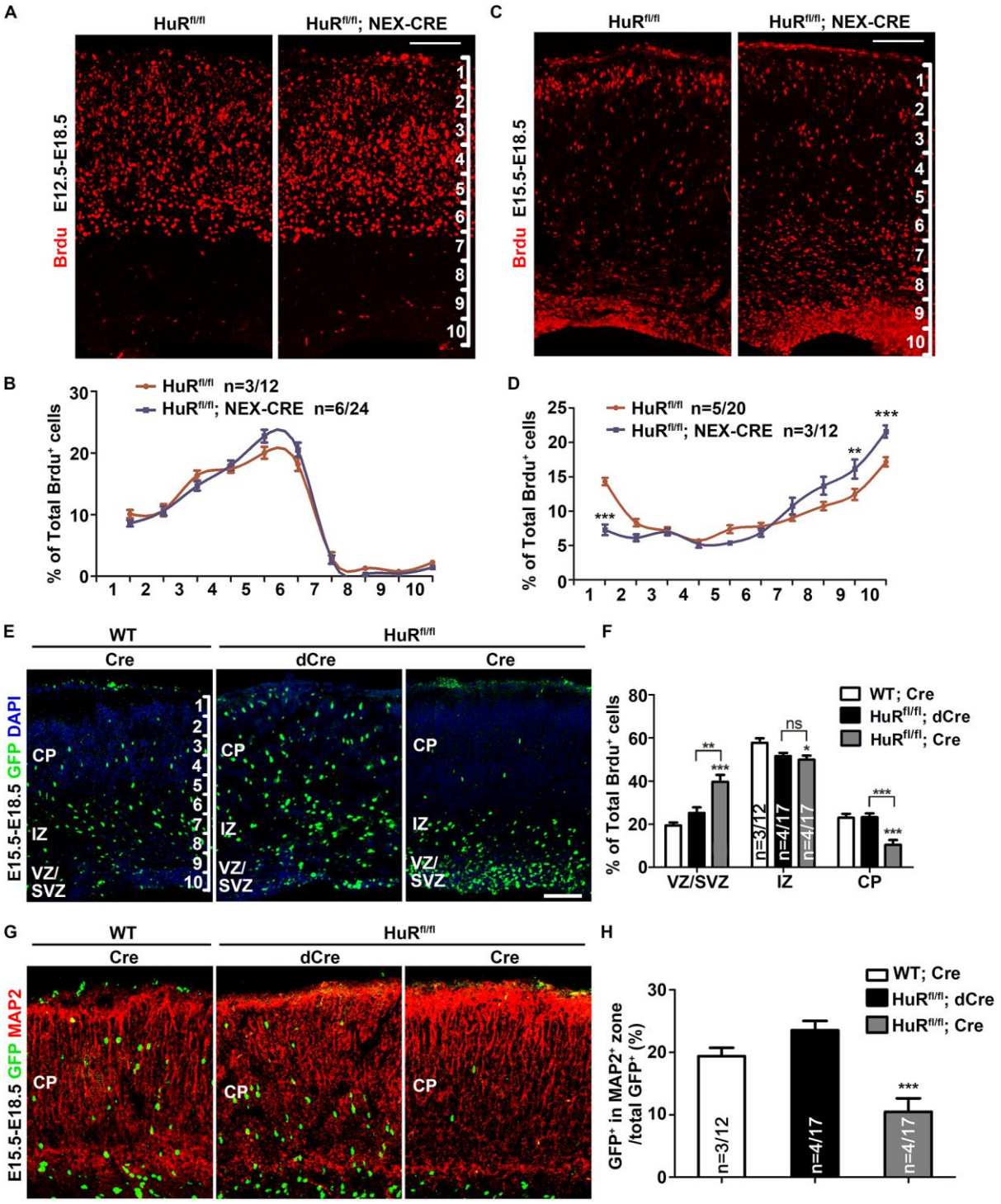

Fig. 2. HuR deficiency impairs the neuronal migration of late-born neurons. (A) Pregnant mice were administered BrdU at E12.5. Coronal sections of each brain were collected at E18.5 and immunostained for BrdU. Cerebral cortices were divided into 10 equal bins. Scale bar=100 μm. (B) Distribution of BrdU$^+$ cells in the cortex of (A). Two-way ANOVA with *Bonferroni* post-hoc analysis was used for statistical analysis. The n values

represent the numbers of brains/brain sections. (C) Pregnant mice were administered BrdU at E15.5. Coronal sections of each brain were collected at E18.5 and immunostained for BrdU. Cerebral cortices were divided into 10 equal bins. Scale bar=100 μm. (D) Distribution of $BrdU^+$ cells in the cortex of (C). Two-way ANOVA with *Bonferroni* post-hoc analysis was used for statistical analysis. The n values represent the numbers of brains/brain sections. (E) GFP-dCre or GFP-Cre plasmids were electroporated into E15.5 $HuR^{fl/fl}$ or WT embryo cortices. Cortical sections were analyzed at E18.5 and immunostained for GFP. Nuclei were counterstained with DAPI. Scale bar=100 μm. (F) Quantification results of GFP^+ neuronal distribution across the cerebral cortex. Fewer GFP^+ neurons were present in the IZ and CP of $HuR^{fl/fl}$; Cre cortical sections. One-way ANOVA with *Bonferroni* post-hoc analysis was performed to analyze the data. The n values represent the numbers of brains/brain sections. (G) dCre or Cre plasmids were electroporated into E15.5 $HuR^{fl/fl}$ or WT embryo cortices. Cortical sections were analyzed at E18.5 and immunostained for GFP and MAP2. (H) Quantification of GFP^+ neuronal distribution in the CP (MAP2 staining zone). One-way ANOVA with *Bonferroni* post-hoc analysis was performed to analyze the data. Scale bar=100 μm. The n values represent the numbers of brains/brain sections. The data show the means ± SEM. n.s.: $P > 0.5$; *: $P < 0.05$; **: $P < 0.01$; ***: $P < 0.001$.

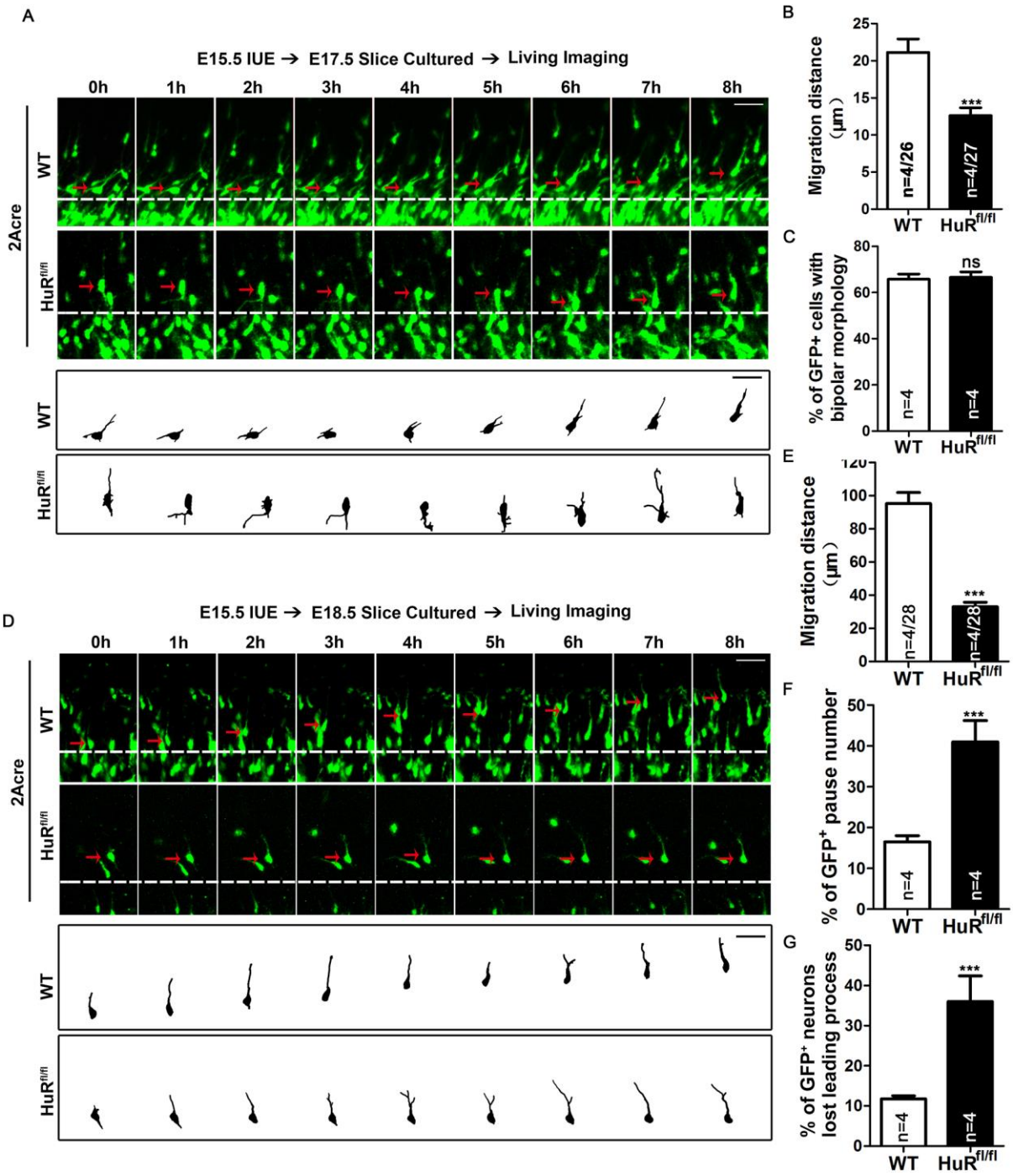

Fig. 3. HuR deficiency impairs the cell motility of migrating neurons. (A) Brain slices were obtained 2 days after *in utero* electroporation of GFP-2A-Cre plasmids into E15.5 $HuR^{fl/fl}$ or WT embryos. An 8-h time-lapse imaging assay was performed for each slice to acquire serial images of migrating neurons in the IZ. Representative neurons are indicated by red arrows, and tracings of each neuron are shown in the lower panels. Scale bars=20 μm. (B) Quantification of migration distance of neurons in (A). Student's t-test was used for statistical

analysis. The n values represent the numbers of brains/neurons. (C) Percentages of GFP^+ neurons in (A) that completed the multipolar-to-bipolar transition during the recording period. Student's t-test was used for statistical analysis. The n values represent the numbers of brains sections. (D) Brain slices were obtained 3 days after *in utero* electroporation of RV-CAG-GFP-2A-Cre plasmids into E15.5 $HuR^{fl/fl}$ or WT embryos. An 8-h time-lapse imaging assay was performed for each slice to acquire serial images of migrating neurons in the CP. Representative neurons are indicated by red arrows, and tracings of each neuron are shown in the lower panels. Scale bars=20 μm. (E) Quantification of migration distance of neurons in (D). Student's t-test was used for statistical analysis. The n values represent the numbers of brains/neurons. (F) Percentage of GFP^+ neurons that did not migrate during the entire recording period in (D). Student's t-test was used for statistical analysis. The n values represent the numbers of brain sections. (G) Percentage of GFP^+ neurons that lost a proper leading process during the recording period in (D). At least 40 GFP^+ neurons were counted in each cortical slice. Student's t-test was used for statistical analysis. The n values represent the numbers of brain sections. Data in this figure are from 4 independent experiments. The numbers of brains, brain sections and neurons quantified in each experiment are indicated on the graphs or in the legend. The data are shown as means ± SEM. Student's t-test was used for statistical analyses in this figure. n.s.: $P > 0.5$; *: $P < 0.05$; **: $P < 0.01$; ***: $P < 0.001$.

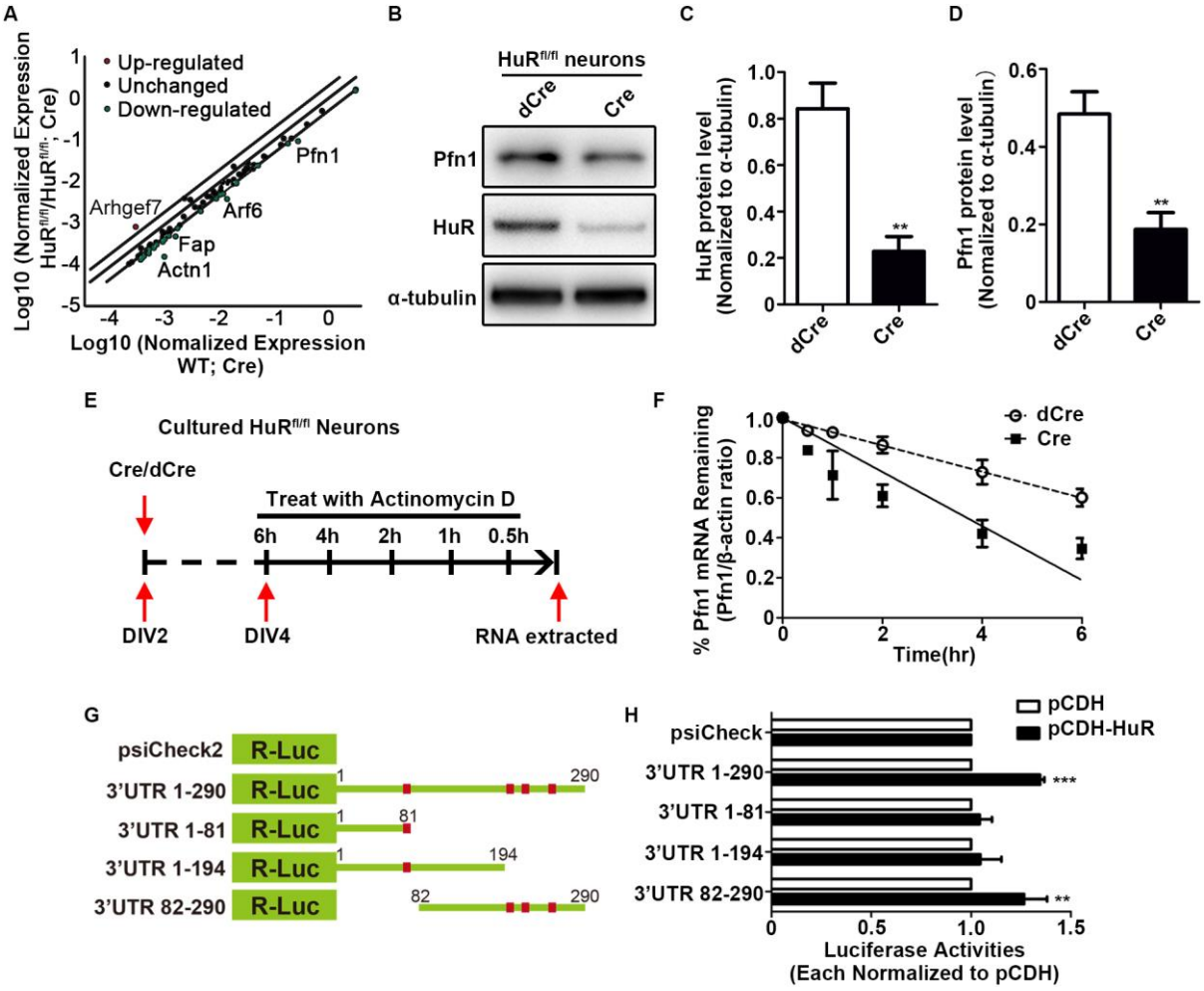

Fig. 4. HuR binds to profilin1 mRNA to promote Profilin1 expression. (A) Scatter plot of PCR array result. Two-fold expression change was selected as the threshold. Up-regulated genes are highlighted in red, and down-regulated genes are highlighted in green. (B) Representative Western blotting analysis of Pfn1 protein expression in $HuR^{fl/fl}$ neurons infected with GFP-Cre or GFP-dCre lentivirus. (C) and (D) Quantitative analyses showed that HuR and Pfn1 expression levels were significantly reduced in GFP-Cre-infected $HuR^{fl/fl}$ neurons. Quantification results were from 3 independent experiments. Student's t-test was used for statistical analysis. (E) Schematic of actinomycin D treatment and RNA extraction of Cre and dCre lentivirus-infected neurons. (F) Slope curve of *pfn1* mRNA metabolism rate. Actinomycin D treatment accelerated *pfn1* mRNA degradation in neurons. (G) Schematic of all constructs of *pfn1* mRNA 3′ UTRs that were used in dual-luciferase reporter assays. (H) R-Luc activities produced by different constructs were normalized to control F-Luc activities in the same psiCheck2 vectors. Luciferase activities in the pCDH-HuR transfected conditions

were compared to the pCDH-transfected conditions. Quantification results are from 4 independent experiments. Student's t-test was used for statistical analysis. The data are shown as means ± SEM. n.s.: $P > 0.5$; *: $P < 0.05$; **: $P < 0.01$; ***: $P < 0.001$.

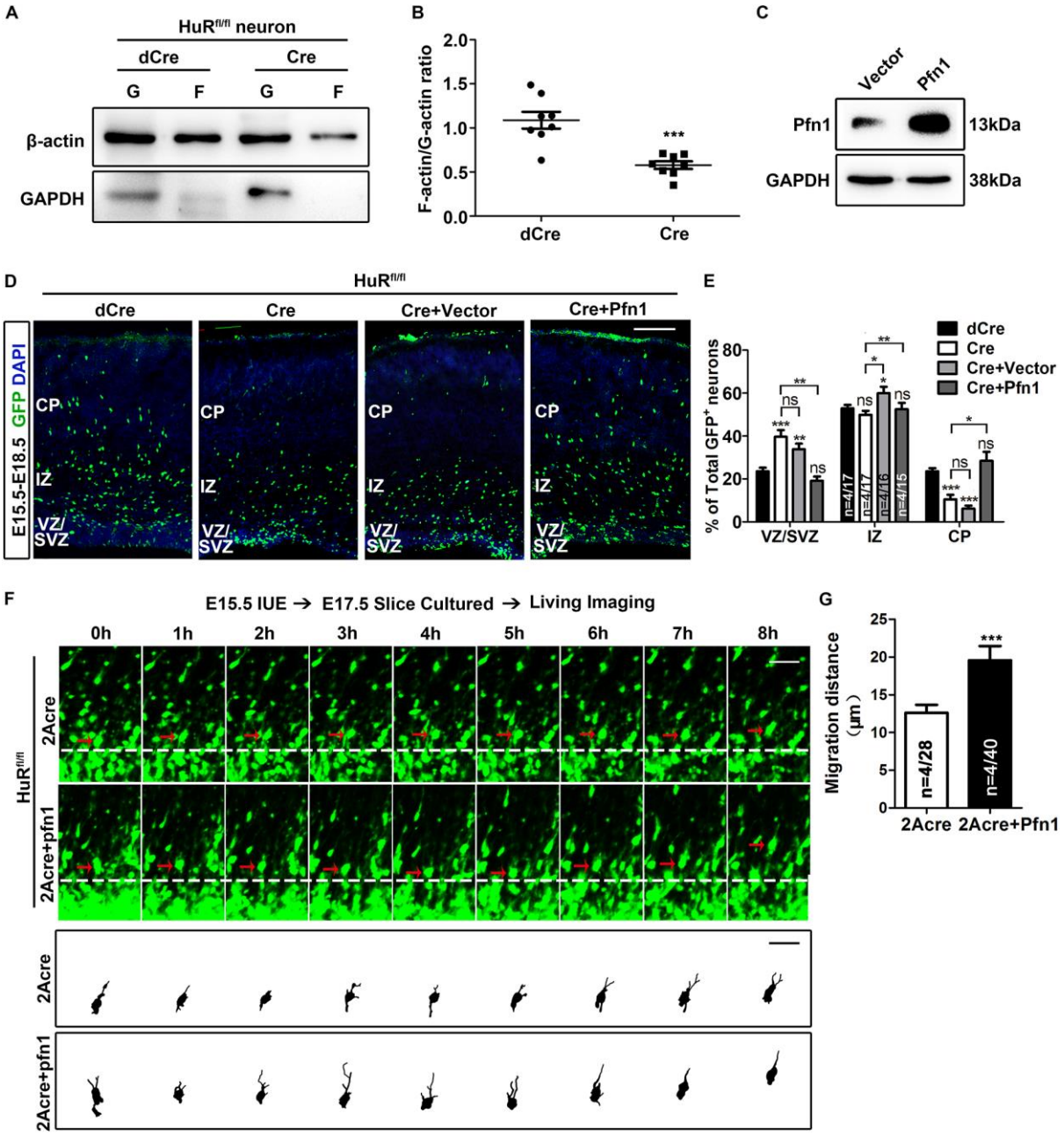

Fig. 5. Profilin1 rescues the neuronal migration defects of HuR-deleted neurons. (A) Western blotting analyses of G-actin and F-actin fractions in cultured $HuR^{fl/fl}$ neurons that infected with dCre and Cre lentivirus. The fraction of F-actin was obviously decreased in HuR-deleted neurons. (B) Quantification of G/F-actin ratio as determined using densitometry analyses of Western blotting results from 4 independent experiments run in duplicate. Mann-Whitney U was used for statistical analysis. (C) NLT cells were transfected with the indicated plasmids. Cell lysates were incubated with an anti-Pfn1 antibody to detect the overexpression of Pfn1. NAPDH was used as a loading control. (D) E15.5 $HuR^{fl/fl}$ embryonic brains were

electroporated with the indicated plasmids, and cortical slices were stained with an anti-GFP antibody and DAPI at E18.5. The mole ratio of Cre vector to Pfn1 expression vector is 1:1. Scale bar=100 μm. (E) Quantification analyses of GFP^+ neuron distribution in (D). One-way ANOVA with *Bonferroni* post-hoc analysis was performed to analyze the data. The n values represent the numbers of brains/brain sections. (F) Brain slices were obtained 2 days after *in utero* electroporation of GFP-2A-Cre or GFP-2A-Cre plus Pfn1 plasmids into E15.5 $HuR^{fl/fl}$ embryos. An 8-h time-lapse imaging assay was performed for each slice. Representative neurons are indicated by red arrows, and tracings of each neuron are shown in the lower panels. The mole ratio of 2A-Cre vector to Pfn1 expression vector is 1:1. Scale bars=20 μm. (G) Quantification of migration distance of neurons in (F). Student's t-test was used for statistical analysis. The n values represent the numbers of brains/neurons. The data are shown as means ± SEM. n.s.: $P > 0.5$; *: $P < 0.05$; **: $P < 0.01$; ***: $P < 0.001$.

Supplementary Materials

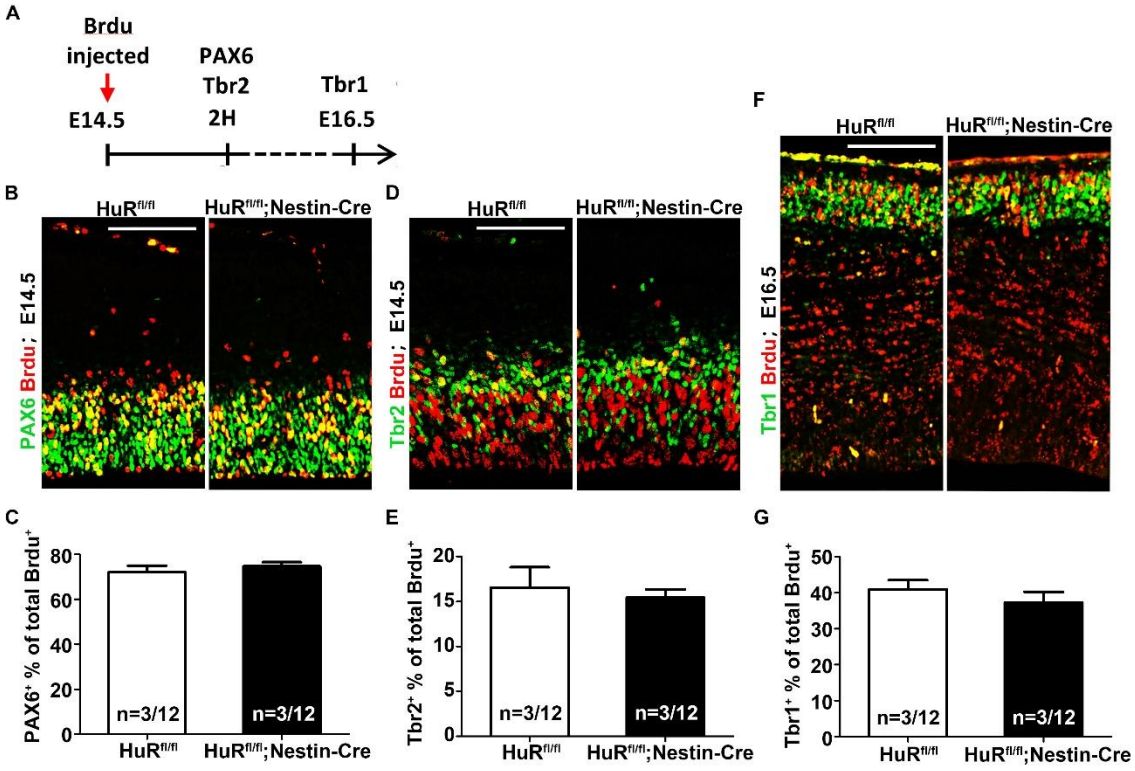

Fig. S1. HuR deletion did not affect neural progenitor cell proliferation or differentiation. (A) Schematic of BrdU labeling assay. (B) BrdU was administrated at E14.5 $HuR^{fl/fl}$; Nestin-Cre mice and $HuR^{fl/fl}$ mice. Brain sections were stained with anti-PAX6 and anti-BrdU antibodies in 2 h post BrdU injection. (C) The ratio of $PAX6^+$ $BrdU^+$ among the total $BrdU^+$ cells was similar between two mice groups. Student's t-test was used for statistical analysis. The n values represent the numbers of brains/brain sections. (D) BrdU was administrated at E14.5 $HuR^{fl/fl}$; Nestin-Cre mice and $HuR^{fl/fl}$ mice. Brain sections were stained with anti-Tbr2 and anti-BrdU antibodies in 2 h post BrdU injection. (E) The ratio of $Tbr2^+$ $BrdU^+$ among the total $BrdU^+$ cells was similar between two mice groups. Student's t-test was used for statistical analysis. The n values represent the numbers of brains/brain sections. (F) BrdU was administrated at E14.5 $HuR^{fl/fl}$; Nestin-Cre mice and $HuR^{fl/fl}$ mice. Brain sections were stained with anti-Tbr1 and anti-BrdU antibodies in 2 h post BrdU injection. (G) The ratio of $Tbr1^+$ $BrdU^+$

among the total BrdU^{+} cells was similar between two mice groups. Student's t-test was used for statistical analysis. The n values represent the numbers of brains/brain sections. The data are shown as means ± SEM. n.s.: P > 0.5; *: P < 0.05; **: P < 0.01; ***: P < 0.001.

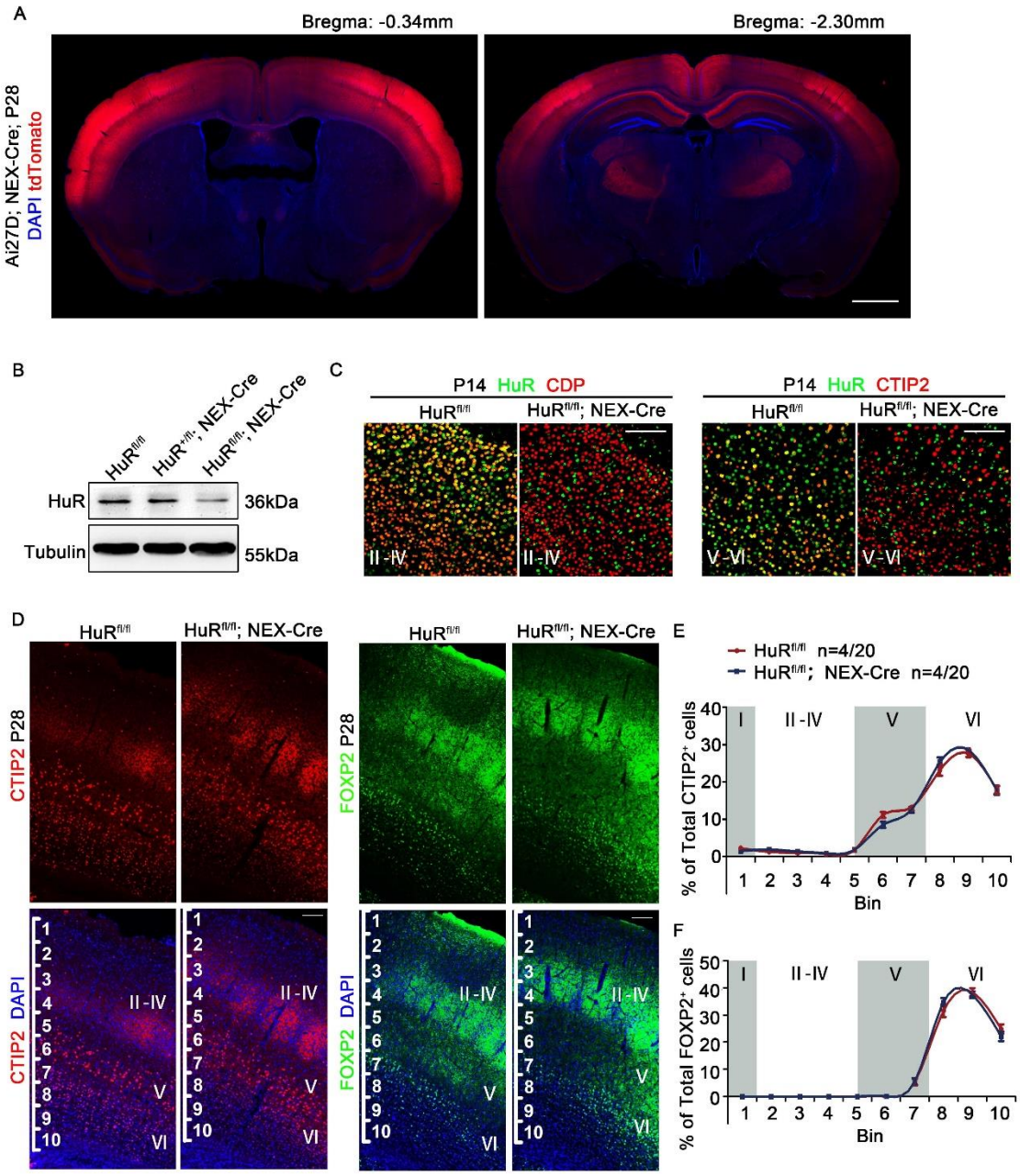

Fig. S2. Deletion of HuR in post-mitotic neurons affects cortical lamination.

(A) Representative images of P28 Ai27D; NEX-Cre cortical sections. The tdTomato signal was present in the cortex and hippocampus. (B) Western blotting analyses of HuR protein expression in P0 HuR$^{fl/fl}$, HuR$^{+/fl}$; NEX-Cre; and HuR$^{fl/fl}$; NEX-Cre

cortical lysates. (C) Immunostaining of CDP, CTIP2 and HuR in P14 $HuR^{fl/fl}$ and $HuR^{fl/fl}$; NEX-Cre cortical sections. HuR was absent from CDP^+ and $CTIP2^+$ cells. Scale bar=100 μm (D) Immunostaining of CTIP2 and FOXP2 in P28 $HuR^{fl/fl}$ and $HuR^{fl/fl}$; NEX-Cre cortical sections. Scale bar=100 μm. (E) Distribution of $CTIP2^+$ neurons in the cortex. Cerebral cortices were divided into 10 equal bins. Two-way ANOVA with *Bonferroni* post-hoc analysis was used for statistical analysis. The n values represent the numbers of brains/brain sections. (F) Distribution of $FOXP2^+$ neurons in the cortex. Cerebral cortices were divided into 10 equal bins. Two-way ANOVA with *Bonferroni* post-hoc analysis was used for statistical analysis. The n values represent the numbers of brains/brain sections. For all images in this figure, nuclei were counterstained with DAPI. The data are shown as means ± SEM. n.s.: $P > 0.5$; *: $P < 0.05$; **: $P < 0.01$; ***: $P < 0.001$.

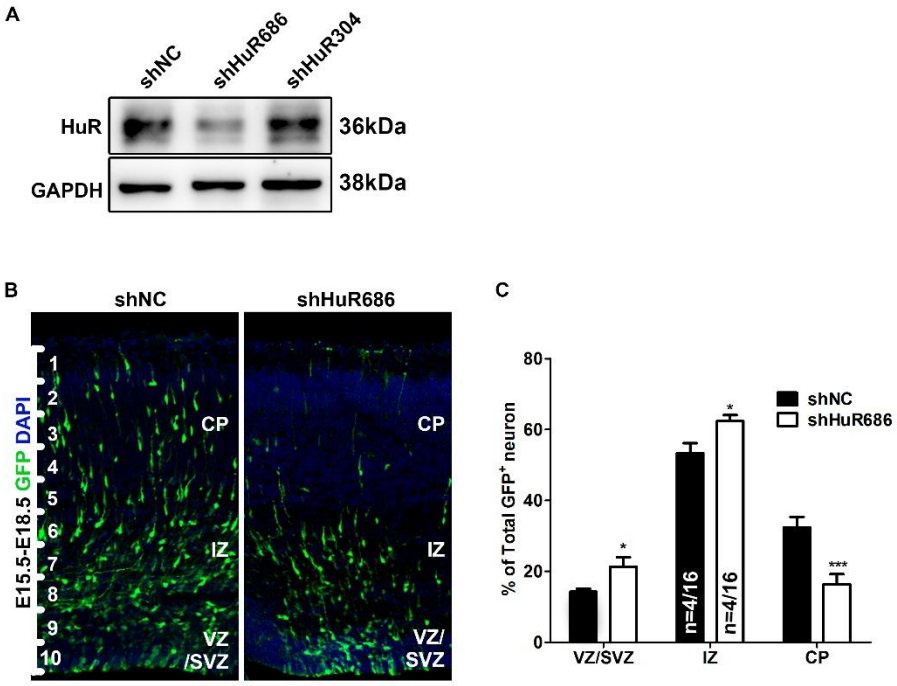

Fig. S3. HuR knockdown impairs neuronal migration. (A) Western blotting analysis showed the knockdown efficiency of shHuR686 was better than that of shHuR304. (B) E15.5 WT embryonic brains were electroporated with indicated plasmids, and cortical slices were stained with an anti-GFP antibody and DAPI at E18.5. Scale bar=100 μm. (C) Cerebral cortices were divided into VZ/SVZ, IZ and

CP areas. Quantification analyses of GFP^+ cells in each area. Student's t-test was used for statistical analysis. The n values represent the numbers of brains/brain sections. The data are shown as means ± SEM. n.s.: P > 0.5; *: P < 0.05; **: P < 0.01; ***: P < 0.001.

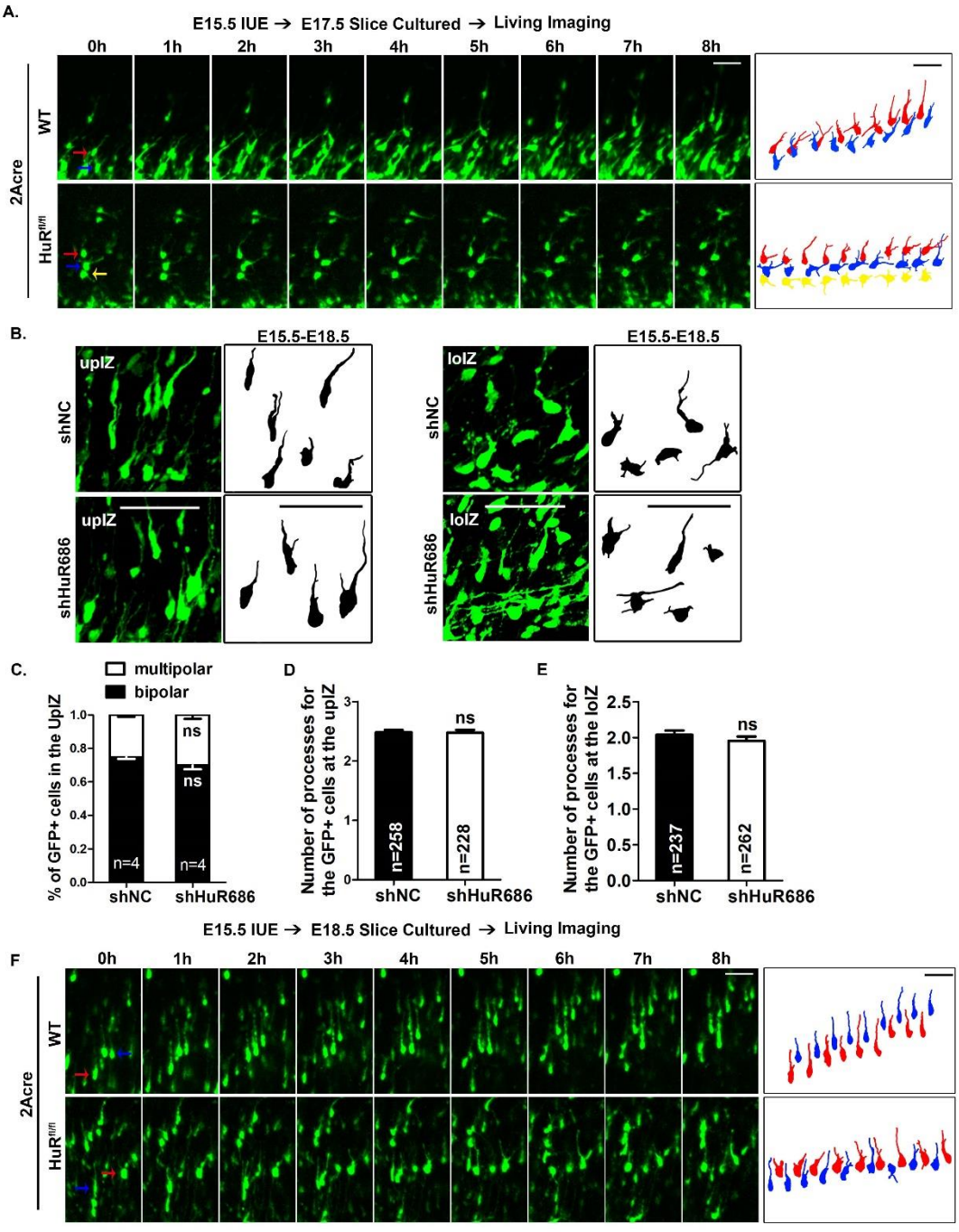

Fig. S4. HuR-deficient neuron exhibits impaired cell motility but normal morphology. (A) Brian slices were obtained 2 days after *in utero* electroporation of

GFP-2A-Cre plasmids into E15.5 $HuR^{fl/fl}$ or WT embryos. An 8-h time-lapse imaging assay was performed for each slice to acquire serial images of migrating neurons in the IZ. Representative neurons are indicated by red, blue and yellow arrows, and tracings of each neuron are shown in the right panels. Scale bars=20 μm. (B) Representative images of GFP^+ neuron in the upIZ and loIZ of brains that were electroporated with indicated plasmids. Scale bars=20 μm. (C) Quantification of multipolar and bipolar neurons in the upIZ of brains that electroporated with indicated plasmids. Student's t-test was used for statistical analysis. The n values represent the numbers of brains. (D) and (E) Quantification of processes of GFP^+ cells in the upIZ and loIZ. Student's t-test was used for statistical analysis. The n values represent the numbers of neurons. (F) Brain slices were obtained 3 days after *in utero* electroporation of RV-CAG-GFP-2A-Cre plasmids into E15.5 $HuR^{fl/fl}$ or WT embryos. An 8-h time-lapse imaging assay was performed for each slice to acquire serial images of migrating neurons in the CP. Representative neurons are indicated by red and blue arrows, and tracings of each neuron are shown in the right panels. Scale bars= 20 μm. The numbers of brains and neurons quantified in each experiment are indicated on the graphs or shown in the legend. The data are shown as means ± SEM. Student's t-test was used for statistical analyses in this figure. n.s.: $P > 0.5$; *: $P < 0.05$; **: $P < 0.01$; ***: $P < 0.001$.

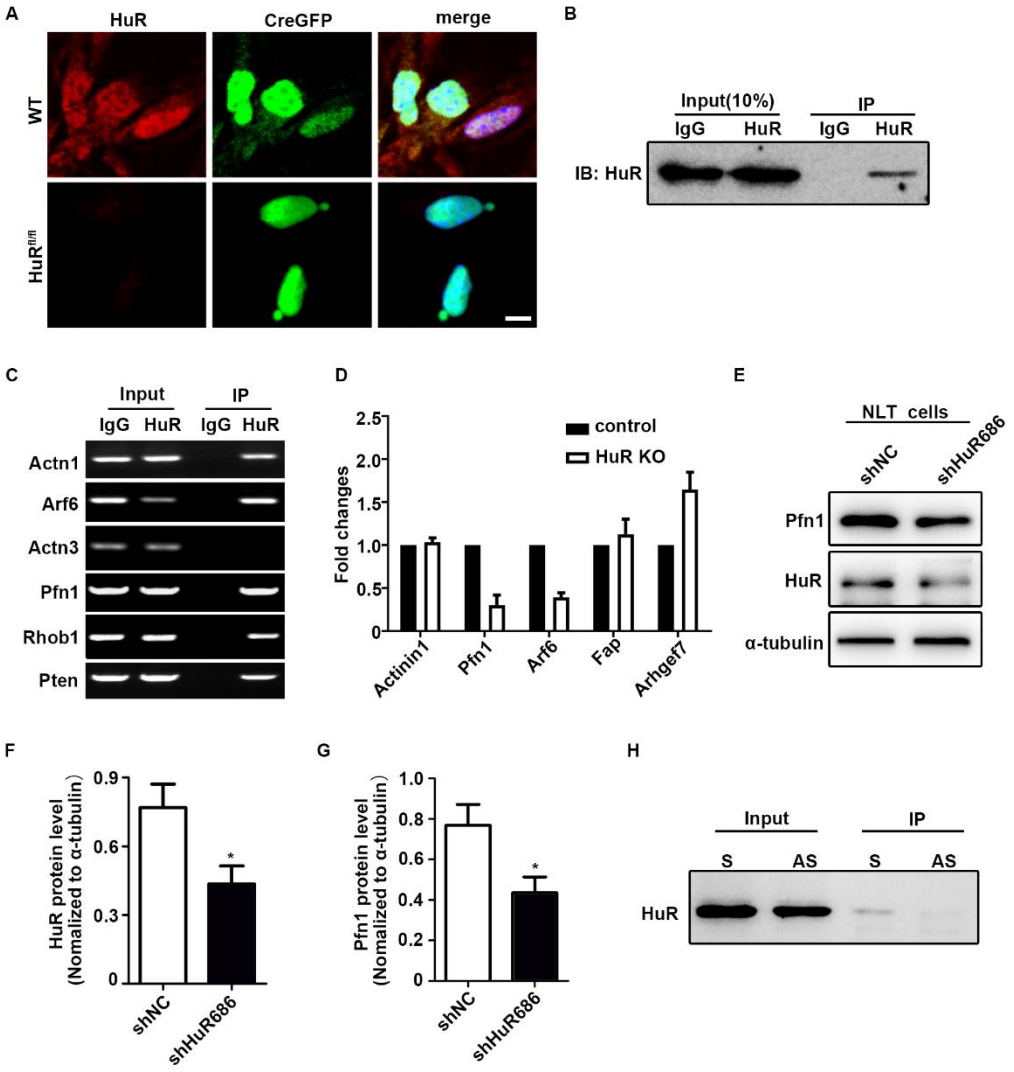

Fig. S5. HuR deficiency impairs Pfn1 expression. (A) Representative images of GFP-Cre lentivirus-infected HuR$^{fl/fl}$ and WT neurons. The absence of HuR staining signal confirmed the deletion of HuR in neurons. (B) RNA-IP using an anti-HuR antibody. (C) RNA-IP of HuR confirmed the binding between HuR protein and the mRNAs of *actn1*, *arf6*, *pfn1*, *rhob1* and *pten*. (D) qPCR analyses of indicated genes that derived from P0 HuR$^{fl/fl}$; Nestin-Cre and HuR$^{fl/fl}$ mice cortical lysates. Mann-Whitney U was used for statistical analysis. Quantification results were from 4 independent experiments. (E) Western blotting analyses of HuR and Pfn1 protein expression in NLT cells that electroporated with shNC or shHuR686 vectors. (F) and (G) Quantitative analyses of HuR (F) and Pfn1 (G) protein expression levels in (E). Quantification results were from

3 independent experiments. Mann-Whitney U was used for statistical analysis. (H) RNA binding assay of *pfn1* mRNA with HuR protein. The sense RNA template of *pfn1* precipitates with HuR protein. Quantification data are shown as means ±SEM. n.s.: P > 0.5; *: P < 0.05; **: P < 0.01; ***: P < 0.001.

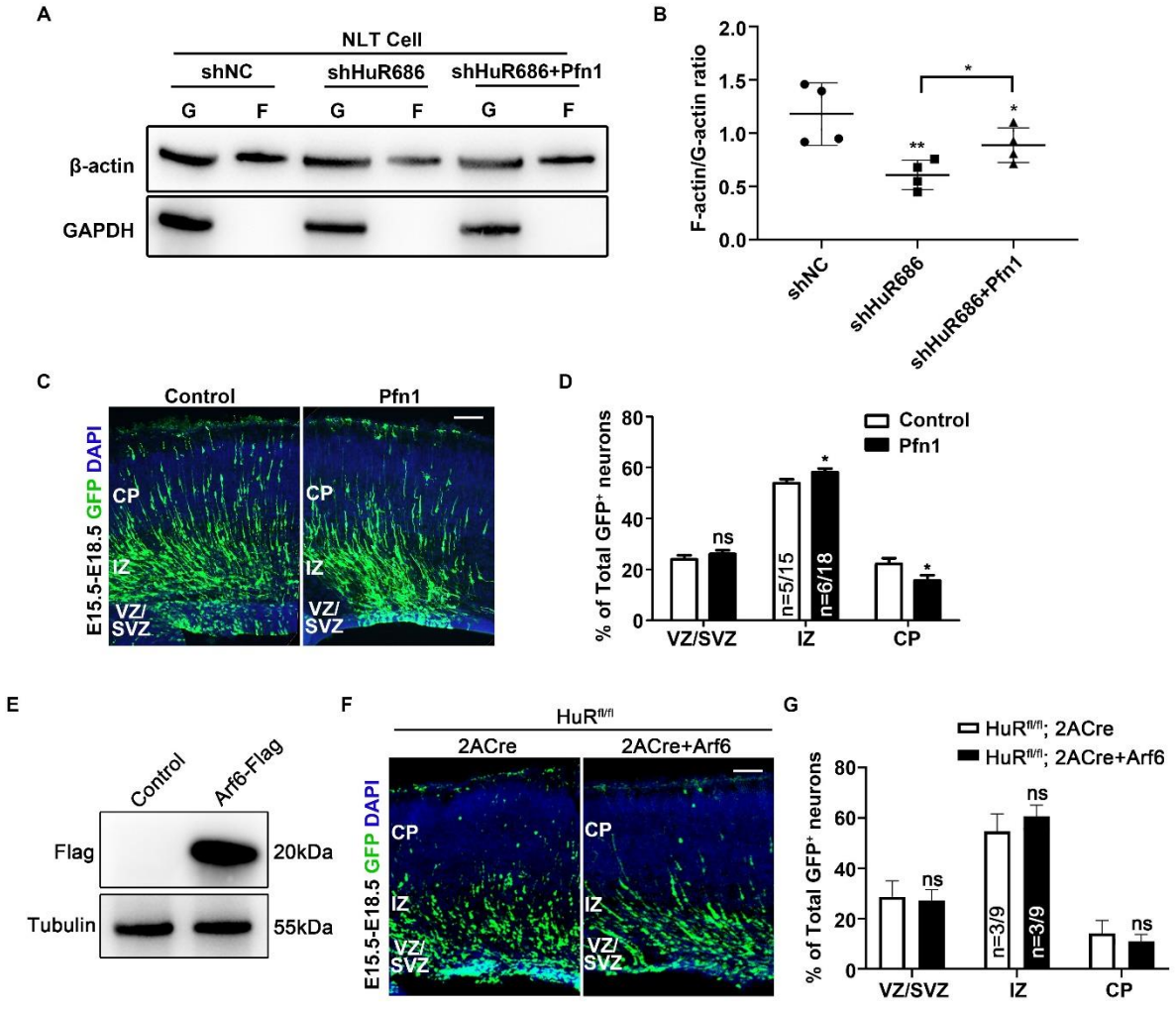

Fig. S6. Pfn1 overexpression rescues migration defects of HuR-deficient neurons. (A) Western blotting analyses of G-actin and F-actin fractions in cultured NLT cells that transfected with indicated plasmid. The mole ratio of shHuR vector to Pfn1 expression vector is 2:1. (B) Quantification of G/F-actin ratio as determined using densitometry analyses of Western blotting results from 4 independent experiments. One-way ANOVA was used for statistical analysis. (C) The control or Pfn1 expression plasmid was electroporated into E15.5 WT embryo cortices. Cortical sections were

analyzed at E18.5 and immunostained for GFP. The nuclei were counterstained with DAPI. Scale bar=100 μm. (D) Quantification results of GFP^+ neuron distribution across the cerebral cortex. Overexpression Pfn1 alone showed a deleterious effect on neuronal migration. Student's t-test was used for statistical analysis. The n values represent the numbers of brains/brain sections. (E) HEK293T cells were transfected with indicated plasmids. Cell lysates were incubated with an anti-Flag antibody to detect the overexpression of Arf6. β-Tubulin was used as a loading control. (F) E15.5 $HuR^{fl/fl}$ embryonic brains were electroporated with the indicated plasmids, and cortical slices were stained with an anti-GFP antibody and DAPI at E18.5. The mole ratio of 2A-Cre vector to Arf6 expression vector is 1:1. Scale bar=100 μm. (G) Quantification analyses of GFP^+ neuron distribution in (F). Student's t-test was used for statistical analysis. The n values represent the numbers of brains/brain sections. The data are shown as means ± SEM. n.s.: $P > 0.5$; *: $P < 0.05$; **: $P < 0.01$; ***: $P < 0.001$.

Table S1 Results of PCR-array

Position	Unigene	GeneBank	Description	Gene Name	Fold of Change	Comment
A01	Mm.489605	NM_026064	*Myl12a*	RIKEN cDNA 2900073G15 gene	-1.92	
A02	Mm.403477	NM_134156	*Actn1*	Actinin, alpha 1	-5.84	#
A03	Mm.5316	NM_013456	*Actn3*	Actinin alpha 3	-2.38	#
A04	Mm.81144	NM_021895	*Actn4*	Actinin alpha 4	-1.21	
A05	Mm.259045	NM_146243	*Actr2*	ARP2 actin-related protein 2 homolog (yeast)	-1.46	
A06	Mm.183102	NM_023735	*Actr3*	ARP3 actin-related protein 3 homolog (yeast)	-1.37	
A07	Mm.6645	NM_009652	*Akt1*	Thymoma viral proto-oncogene 1	1.31	
A08	Mm.27308	NM_007481	*Arf6*	ADP-ribosylation factor 6	-3.52	
A09	Mm.474783	NM_133796	*Arhgdia*	Rho GDP dissociation inhibitor (GDI) alpha	-1.55	
A10	Mm.244068	NM_017402	*Arhgef7*	Rho guanine nucleotide exchange factor (GEF7)	3.04	#
A11	Mm.197534	NM_130862	*Baiap2*	Brain-specific angiogenesis inhibitor 1-associated protein 2	-2.22	
A12	Mm.3758	NM_009954	*Bcar1*	Breast cancer anti-	-1.59	

				estrogen resistance 1		
B01	Mm.6221	NM_007600	*Capn1*	Calpain 1	-2.45	#
B02	Mm.19306	NM_009794	*Capn2*	Calpain 2	-2.00	
B03	Mm.28278	NM_007616	*Cav1*	Caveolin 1, caveolae protein	-2.24	
B04	Mm.447553	NM_009861	*Cdc42*	Cell division cycle 42 homolog (S. cerevisiae)	-2.17	
B05	Mm.329655	NM_007687	*Cfl1*	Cofilin 1, non-muscle	-2.06	
B06	Mm.280125	NM_133656	*Crk*	V-crk sarcoma virus CT10 oncogene homolog (avian)	-1.74	
B07	Mm.795	NM_007778	*Csf1*	Colony stimulating factor 1 (macrophage)	-1.87	#
B08	Mm.490123	NM_007803	*Cttn*	Cortactin	-1.99	#
B09	Mm.195916	NM_007858	*Diap1*	Diaphanous homolog 1 (Drosophila)	-2.26	#
B10	Mm.1151	NM_010074	*Dpp4*	Dipeptidylpeptidase 4	-2.04	#
B11	Mm.252481	NM_010113	*Egf*	Epidermal growth factor	-1.89	#
B12	Mm.420648	NM_007912	*Egfr*	Epidermal growth factor receptor	-1.67	#
C01	Mm.389224	NM_010135	*Enah*	Enabled homolog (Drosophila)	-1.46	
C02	Mm.277812	NM_009510	*Ezr*	Ezrin	-1.44	
C03	Mm.41816	NM_007986	*Fap*	Fibroblast activation protein	-3.10	#

C04	Mm.473689	NM_008006	*Fgf2*	Fibroblast growth factor 2	-2.16	#
C05	Mm.267078	NM_010427	*Hgf*	Hepatocyte growth factor	-2.27	#
C06	Mm.268521	NM_010512	*Igf1*	Insulin-like growth factor 1	-2.29	#
C07	Mm.275742	NM_010513	*Igf1r*	Insulin-like growth factor I receptor	-1.59	
C08	Mm.274846	NM_010562	*Ilk*	Integrin linked kinase	-1.19	
C09	Mm.31903	NM_010576	*Itga4*	Integrin alpha 4	-1.58	#
C10	Mm.263396	NM_010578	*Itgb1*	Integrin beta 1 (fibronectin receptor beta)	-1.69	
C11	Mm.1137	NM_008404	*Itgb2*	Integrin beta 2	-2.49	#
C12	Mm.87150	NM_016780	*Itgb3*	Integrin beta 3	-2.38	#
D01	Mm.15409	NM_010717	*Limk1*	LIM-domain containing, protein kinase	-1.97	#
D02	Mm.196581	NM_011949	*Mapk1*	Mitogen-activated protein kinase 1	-2.06	
D03	Mm.86844	NM_008591	*Met*	Met proto-oncogene	-1.96	#
D04	Mm.486486	NM_008608	*Mmp14*	Matrix metallopeptidase 14 (membrane-inserted)	-1.29	
D05	Mm.29564	NM_008610	*Mmp2*	Matrix metallopeptidase 2	-1.63	#
D06	Mm.4406	NM_013599	*Mmp9*	Matrix	-1.35	#

				metallopeptidase 9		
D07	Mm.138876	NM_010833	*Msn*	Moesin	-1.42	
D08	Mm.218233	NM_175260	*Myh10*	Myosin, heavy polypeptide 10, non-muscle	-1.39	
D09	Mm.29677	NM_022410	*Myh9*	Myosin, heavy polypeptide 9, non-muscle	-1.53	
D10	Mm.33360	NM_139300	*Mylk*	Myosin, light polypeptide kinase	-1.90	#
D11	Mm.260227	NM_011035	*Pak1*	P21 protein (Cdc42/Rac)-activated kinase 1	-1.58	
D12	Mm.21876	NM_027470	*Pak4*	P21 protein (Cdc42/Rac)-activated kinase 4	-1.69	
E01	Mm.2647	NM_011072	*Pfn1*	Profilin 1	-2.96	
E02	Mm.260521	NM_008839	*Pik3ca*	Phosphatidylinositol 3-kinase, catalytic, alpha polypeptide	-1.76	
E03	Mm.1359	NM_011113	*Plaur*	Plasminogen activator, urokinase receptor	-1.66	#
E04	Mm.44463	NM_021280	*Plcg1*	Phospholipase C, gamma 1	-1.54	
E05	Mm.212039	NM_008875	*Pld1*	Phospholipase D1	-1.44	#
E06	Mm.222178	NM_011101	*Prkca*	Protein kinase C, alpha	-1.50	
E07	Mm.245395	NM_008960	*Pten*	Phosphatase and	1.82	

				tensin homolog		
E08	Mm.254494	NM_007982	*Ptk2*	PTK2 protein tyrosine kinase 2	-1.31	
E09	Mm.21613	NM_172498	*Ptk2b*	PTK2 protein tyrosine kinase 2 beta	-1.93	#
E10	Mm.277916	NM_011201	*Ptpn1*	Protein tyrosine phosphatase, non-receptor type 1	-1.80	
E11	Mm.18714	NM_011223	*Pxn*	Paxillin	-1.37	#
E12	Mm.469963	NM_009007	*Rac1*	RAS-related C3 botulinum substrate 1	-1.55	
F01	Mm.1972	NM_009008	*Rac2*	RAS-related C3 botulinum substrate 2	-1.92	#
F02	Mm.259653	NM_145452	*Rasa1*	RAS p21 protein activator 1	-1.92	
F03	Mm.472057	NM_009041	*Rdx*	Radixin	-1.50	
F04	Mm.406156	NM_145383	*Rho*	Rhodopsin	-1.87	#
F05	Mm.318359	NM_016802	*Rhoa*	Ras homolog gene family, member A	-1.66	
F06	Mm.687	NM_007483	*Rhob*	Ras homolog gene family, member B	1.33	
F07	Mm.262	NM_007484	*Rhoc*	Ras homolog gene family, member C	-1.65	
F08	Mm.46497	NM_028810	*Rnd3*	Rho family GTPase 3	-1.82	
F09	Mm.6710	NM_009071	*Rock1*	Rho-associated coiled-coil containing protein kinase 1	-2.04	
F10	Mm.127560	NM_008018	*Sh3pxd2a*	SH3 and PX domains 2A	-1.63	#

F11	Mm.22845	NM_009271	*Src*	Rous sarcoma oncogene	-1.79	#
F12	Mm.249934	NM_011486	*Stat3*	Signal transducer and activator of transcription 3	-1.71	
G01	Mm.136791	NM_153153	*Svil*	Supervillin	-1.78	
G02	Mm.248380	NM_011577	*Tgfb1*	Transforming growth factor, beta 1	-2.51	#
G03	Mm.206505	NM_011594	*Timp2*	Tissue inhibitor of metalloproteinase 2	-2.19	
G04	Mm.208601	NM_011602	*Tln1*	Talin 1	-2.08	
G05	Mm.9684	NM_009499	*Vasp*	Vasodilator-stimulated phosphoprotein	-1.87	#
G06	Mm.279361	NM_009502	*Vcl*	Vinculin	-2.15	
G07	Mm.282184	NM_009505	*Vegfa*	Vascular endothelial growth factor A	-1.73	
G08	Mm.268000	NM_011701	*Vim*	Vimentin	-1.98	
G09	Mm.41353	NM_031877	*Wasf1*	WASP family 1	-1.59	
G10	Mm.23566	NM_153423	*Wasf2*	WAS protein family, member 2	-1.76	#
G11	Mm.1574	NM_028459	*Wasl*	Wiskott-Aldrich syndrome-like (human)	-1.74	
G12	Mm.223504	NM_153138	*Wipf1*	WAS/WASL interacting protein family, member 1	-2.14	#
H03	Mm.304088	NM_008084	*Gapdh*	Glyceraldehyde-3-	1.44	internal

				phosphate dehydrogenase		control
H05	Mm.2180	NM_008302	*Hsp90ab1*	Heat shock protein 90 alpha (cytosolic), class B member 1	-1.44	Internal control

Gene expression was analyzed by Qiagen online software (https://www.qiagen.com/cn/shop/genes-and-pathways/data-analysis-center-overview-page/) using Gapdh and Hsp90ab1 as internal control. Up-regualted genes were shown as positive values and down-regulated genes were shown as negative values. # indicated genes that had low basal expression level (Ct value>30 in control samples). The most up-regulated gene (*Arhgef7*) was colored in RED, and the most down-regulated genes (*Actn1*, *Arf6*, *Fap*, *Pfn1*) were colored in GREEN.

Table S2 Sequences of primers in this study

Primers	Sequence 5' to 3'	Notes
NEX Cre 1：	CCGCATAACCAGTGAAACAG	(Goebbels et al., 2006)
NEX Cre 2：	AGAATGTGGAGTAGGGTGAC	Pair with NEX Cre 1
NEX Cre 3：	GAGTCCTGGCAGTCTTTTTC	Pair with NEX Cre 1
HuR flox F：	CTCTCCAGGCAGATGAGCA	(Ghosh et al., 2009)
HuR flox R：	TAGGCTCTGGGATGAAACCT	
Ai27D Wild F：	AAG GGA GCT GCA GTG GAG TA	(Linda et al., 2012)
Ai27D Wild R：	CCGAAAATCTGTGGGAAGTC	
Ai27D Mutant F：	CTGTTCCTGTACGGCATGG	(Linda et al., 2012)
Ai27D Mutant R:	GGCATTAAAGCAGCGTATCC	
Nestin-Cre 1:	GCCTTATTGTGGAAGGAC	(Giusti et al., 2014)
Nestin-Cre 2:	TTGCTAAAGCGCTACATAGGA	Pair with Nestin-Cre 1
Nestin-Cre 3	CCTTCCTGAAGCAGTAGAGCA	Pair with Nestin-Cre 1
1-81 3'UTR: F:	CCGCTCGAGCCTCATCTGTCCCTTCCCCCCACCG	Pfn1 cloning
1-81 3'UTR: R:	TTTTCCTTTTGCGGCCGCAAAAAATAATGGTATGTGTG	Pfn1 cloning
82-290 3'UTR: F:	CCGCTCGAGGGGCCATTACCCCATTTC	Pfn1 cloning
82-290 3'UTR: R:	TTTTCCTTTTGCGGCCGCTTTTTTTTTTTTTTTGTTAG	Pfn1 cloning
1-194 3'UTR: R:	TTTTCCTTTTGCGGCCGCTTTTCCAAACACACACAGGA	Pfn1 cloning
HuR F：	TTCTGGTGTCAATGTCCCCG	qPCR
HuR R：	CAAAGGGGCCAAACATCTGC	qPCR
GAPDH F：	GAGAGACCCTCACTGCTG	qPCR
GAPDH R：	GATGGTACATGACAAGGTGC	qPCR
Profilin1 F：	GTGGAACGCCTACATCGACA	qPCR

Profilin1 R：	TTGACCGGTCTTTGCCTACC	qPCR
Actn1 F：	ACATGCAGCCTGAAGAGGAC	qPCR
Actn1 R：	TGAGATGACCTCCAGGAGCA	qPCR
Arf6 F：	ATCTTCGCCAACAAGCAGGA	qPCR
Arf6 R：	AGGTTAACCATGTGAGCCCC	qPCR
Actn3 F：	GAGCTCGACTACCATGAGGC	qPCR
Actn3 R：	GCCAGTTATTGAAGGGGGCT	qPCR
Rhob F：	ACTATGTGGCGGACATCGAG	qPCR
Rhob R：	AGAAGTGCTTTACCTCGGGC	qPCR
Pten F：	TCCTGCAGAAAGACTTGAAGGT	qPCR
Pten R：	GCTGTGGTGGGTTATGGTCT	qPCR
Fap F:	GGCTGGGGCTAAGAATCCG	qPCR
Fap R:	GCATACTCGTTCACTGGACAC	qPCR
Arhgef7 F:	CATAATCACGTCTTGGCTGATGA	qPCR
Arhgef7 R	CAGCAGCTCTTACGGGATGC	qPCR
pfn1-F	CCTCATCTGTCCCTTCCCCCCACCG	RNA binding assay
pfn1-R	GTTAGTAGAATCTTTTTTTATTCAGAAAAA	RNA binding assay